nature communications

Article

https://doi.org/10.1038/s41467-024-50985-8

Cxcr4 regulates a pool of adipocyte progenitors and contributes to adiposity in a sex-dependent manner

Received: 10 August 2022

Accepted: 26 July 2024

Published online: 05 August 2024

Check for updates

Benjamin M. Steiner[1,3], Abigail M. Benvie[1,3], Derek Lee[1,3], Yuwei Jiang[2] & Daniel C. Berry[1]

Sex steroids modulate the distribution of mammalian white adipose tissues. Moreover, WAT remodeling requires adipocyte progenitor cells. Nevertheless, the sex-dependent mechanisms regulating adipocyte progenitors remain undetermined. Here, we uncover Cxcr4 acting in a sexually dimorphic manner to affect a pool of proliferating cells leading to restriction of female fat mass. We find that deletion of *Cxcr4* in *Pparγ*-expressing cells results in female, not male, lipodystrophy, which cannot be restored by high-fat diet consumption. Additionally, *Cxcr4* deletion is associated with a loss of a pool of proliferating adipocyte progenitors. *Cxcr4* loss is accompanied by the upregulation of estrogen receptor alpha in adipose-derived PPARγ-labelled cells related to estradiol hypersensitivity and stalled adipogenesis. Estrogen removal or administration of antiestrogens restores WAT accumulation and dynamics of adipose-derived cells in *Cxcr4*-deficient mice. These findings implicate Cxcr4 as a female adipogenic rheostat, which may inform strategies to target female adiposity.

Mammalian white adipose tissue (WAT) regulates appetite, sexual reproduction, metabolic responses, thermoregulation, and energy storage[1,2]. Yet, excess fat mass—obesity—is associated with a disturbance in metabolic stability, placing WAT as a central regulator for determining overall health in response to overnutrition[3]. But overall, adiposity may not be a direct correlate to metabolic health. For example, individuals with similar body mass index (BMI)—the current matrix used to determine obesity—may not have the same propensity to develop metabolic or cardiovascular diseases[4,5]. This outcome could be partly attributed to genetics but may also reflect body fat distribution and placement[6]. This is because WAT can be broadly subdivided into subcutaneous fat, residing under the skin, and visceral fat, located within the visceral cavity, which are responsive to changes in energy balance. Unequivocally, an accumulation and expansion of visceral adiposity with a subsequent loss in subcutaneous fat increases an individual's risk of developing metabolic disease and premature death[7,8]. Conversely, subcutaneous fat growth, per se, is metabolically protective due to its role in insulin sensitization, anti-inflammatory properties, and adipogenic potential[9–11].

In several regards, gonadal steroids (i.e., estrogen and testosterone) mediate body fat storage into subcutaneous and visceral compartments[6,12–14]. For instance, even though women tend to have more total fat than men, females have more metabolically protective subcutaneous fat. In contrast, males tend to have more visceral fat, augmenting metabolic dysregulation and cardiometabolic disease[7]. Correspondingly, in postmenopausal women—the decline of circulating estrogens—there is an increase in visceral adiposity, a regression of protective subcutaneous fat, an impairment in insulin signaling, and oscillations in body temperature[15,16]. Estrogen hormone replacement therapy (HRT) can counteract or alleviate some postmenopausal metabolic perturbations[17]. For instance, estrogen can regulate adiposity and metabolic responses in both females and males, and this action appears to derive from a diverse biological effect in various tissue types such as adipocytes, neurons, and the hypothalamus[18–22].

[1]Division of Nutritional Sciences, Cornell University, Ithaca, NY 14853, USA. [2]Department of Physiology and Biophysics, University of Illinois at Chicago, Chicago, IL 60612, USA. [3]These authors contributed equally: Benjamin M. Steiner, Abigail M. Benvie, Derek Lee. e-mail: dcb37@cornell.edu

Estrogen's biological actions are mediated by estrogen receptors (ER) α and β, a class of ligand-dependent nuclear hormone receptors that regulate gene transcription[23,24]. Several genetic studies have implicated ER activity within the central nervous system as a primary mediator of estrogen-induced metabolic responses[20]. In contrast, other studies have demonstrated the requirement of ER signaling in mature adipocytes to regulate adipocyte hypertrophy and WAT inflammation and fibrosis[19,25]. More recently, ER signaling has been shown to be critical for white adipocyte lineage regulation and adipocyte maturation[26]. Current evidence suggests that estrogen action blocks adipogenesis, yet our understanding of the molecular signals modulating ER activity and expression under the adipogenic context, is unclear[27,28].

Fat tissue remodeling has been primarily linked to adipocyte hypertrophy. However, recent studies have suggested that changes in adiposity may reflect changes in adipocyte number rather than solely enlargement[29,30]. Like several adult tissues, WATs contain resident adipocyte progenitor cells (APCs) capable of generating new adipocytes under homeostatic conditions and obesogenic expansion[31–33]. The critical driver of new adipocytes is peroxisome proliferator activated receptor gamma (Pparγ)[31,34,35]. While Pparγ is expressed in a number of cell types, including macrophages, monocytes, endothelial cells, smooth muscle cells, it is also expressed within a subset of adult APCs[31,36–39]. APCs also express mural cell markers and reside along the WAT vasculature, which serves as the APC niche[40–42]. Notably, the niche serves as a central regulatory node directing progenitor cell function and dynamics to preserve tissue homeostasis and function[43]. This notion positions the niche as a bi-directional regulator of stem cell function and tissue regulation[44]. Additionally, distinct proliferative and differentiation responses exist between male and female tissues and niches. For example, sex-dependent changes in APC dynamics directly affect body fat distribution and growth and metabolic outcomes[45]. However, the factors responsible for transducing sex-dependent changes within APCs and coordinating adipose tissue mass remain unknown. Interestingly, a recent study demonstrated the critical role of the chemokine receptor, Cxcr2, to regulate adipocyte development in a sex-dependent manner[46]. Cxcr2 knockout (KO) mice exhibited a thinner subcutaneous layer, smaller adipocytes, and reduced expression of adipogenic genes. Notably, these changes were more pronounced in female Cxcr2-KO mice compared to male mutant mice[46]. This evidence points to an important sex-specific influence of Cxcr2 and potentially other chemokine receptors on adipose tissue regulation and metabolic health.

In this study, we reveal another chemokine receptor, C-X-C motif chemokine receptor 4 (*Cxcr4)* acting as a mediator of sexual dimorphic adiposity. Interestingly, *Cxcr4* expression is enriched in *Pparγ*-labelled cells in female adipose tissue compared to males. Deleting *Cxcr4* within *Pparγ*-marked cells results in female lipodystrophy, which cannot be restored in response to HFD. Moreover, the loss of *Cxcr4* is associated with the exhaustion of proliferating Pparγ-labelled cells in adipose tissue and a shift to a more quiescent state. Mechanistically, *Cxcr4*-deficient adipose derived-Pparγ-labelled cells overexpress ERα and are highly sensitive to estrogen bioavailability, thereby inhibiting adipogenesis. Correspondingly, blocking ERα activity with antiestrogens or reducing circulating estrogen by ovariectomy (OVX) results in adipogenic restoration.

Results

Cxcr4 is expressed in mature adipocytes

Broadly, subcutaneous and visceral WAT have different metabolic processes, developmental origins, and endocrine functions[47]. While evaluating differential effectors between subcutaneous and visceral fat, we found that *Cxcr4* mRNA expression was enriched in visceral gonadal WAT (gWAT) of male and female mice compared to subcutaneous inguinal WAT (iWAT) (Fig. 1a). Upon further evaluation, *Cxcr4* mRNA expression was elevated in isolated floated adipocytes compared to lineage-negative (Lin-negative; Cd45-, Cd31-) stromal vascular (SV) cells in both iWAT and gWAT samples from male and female mice (Fig. 1b, c). *Cxcr4* adipocyte enrichment suggested this receptor may increase in response to in vitro SV cell adipogenic induction. Indeed, *Cxcr4* gene expression increased with adipogenic media and adipocyte formation, mirroring *Pparγ* expression[35], suggesting that *Cxcr4* may be involved in the adipogenic program (Fig. 1d).

Cxcr4 is dispensable for mature adipocyte function

Given that *Cxcr4* is expressed in the adipocyte compartment, we first investigated if Cxcr4 has a role in mature adipocytes. Notably, previous work using a *Fabp4*-Cre mouse model to delete *Cxcr4*, has posited that Cxcr4 may control mature adipocyte function[48]. However, the *Fabp4*-Cre model does not allow for appropriate adipocyte penetrance and selectivity[49]. Therefore, we combined the $Cxcr4^{fl/fl}$ mouse model with the adipocyte-specific Cre driver mouse model, *Adiponectin*-Cre[50], to create $Cxcr4^{AdipoQ}$KO mice (*Adiponectin*-Cre; $Cxcr4^{fl/fl}$). Phenotypically, at postnatal day (P) 60 (P60), male and female control and mutant mice appeared comparable in body weight, glucose clearance, and adiposity (Supplementary Fig. 1a–c and Supplementary Fig. 2a–c). Histologically, iWAT and gWAT sections from male and female controls and mutants appeared similar in adipocyte size and architecture. Fibrotic and inflammatory staining also revealed comparable presence (Supplementary Fig. 1d–i and Supplementary Fig. 2d–i). These data were further supported by gene expression analysis of adipocyte, fibrotic, and inflammatory markers (Supplementary Fig. 1j–o and Supplementary Fig. 2j–o). Overall, Cxcr4 function, under physiological conditions, may be unnecessary for adipocyte maturation and function.

Cxcr4 is enriched within the female *Pparγ* labelled adipose tissue

Because Cxcr4 signaling and GTPase activity can regulate stem cell dynamics[51], we turned our attention back to SV cells and assessed *Cxcr4* expression by flow cytometry. To detect adipogenic cells, we employed the AdipoTrak adipose lineage tracking mouse model, which incorporates a doxycycline-suppressible tetracycline-controlled transactivator (tTA) knocked into the endogenous locus of *Pparγ*[31]. Further, we combined the AdipoTrak system with the proliferative marker TRE-H2B-GFP to visualize *Pparγ*-marked cells (Supplementary Fig. 3a–g). Notably, AdipoTrak-marked cells have been shown to mark the entire adipose lineage (stem-to-adipocyte) and are required for fat development and homeostasis[41,52]. However, *Pparγ* is known to be expressed in other cell types, including macrophages, monocytes, endothelial cells, and smooth muscle cells[35–39]. Consistent with expression in adipose tissue, adipogenic assays revealed that all in vitro-derived adipocytes from male and female iWAT depots develop from a FACS-isolated GFP^{AT+} population (Supplementary Fig. 3h–k). As a next step, we performed flow cytometric analysis on GFP^{AT+} cells for Dpp4 and Pdgfrα−adipose lineage markers−from the total SV cell compartment from iWAT and gWAT depots from male and female mice (Supplementary Fig. 4a–e). Indeed, both Dpp4 and Pdgfrα individually overlapped with the GFP^{AT} marker, suggesting that identified adipose lineage markers label AdipoTrak cells (Supplementary Fig. 5a–r). Specifically, we found that about 40% and 60% of the AdipoTrak cell population was marked by Pdgfrα and Dpp4, respectively. We also evaluated the reverse, the percentage of GFP^{AT+} labeling within the total Dpp4 and Pdgfrα individual populations. Again, we found considerable overlap between AdipoTrak and Dpp4 and Pdgfrα individual populations, but these percentages varied depending on sex and depot (Supplementary Fig. 5a–r). To further understand the lineage relevance of AdipoTrak-marked cells, we interrogated the doubly labeled Dpp4 and Pdgfrα cells for GFP^{AT+} co-expression in iWAT and gWAT depots in male and female mice. Interestingly, the overlap of all three markers represented about 20-30% of the total pool of triply

labeled cells, suggesting these markers may represent various stages of adipogenic commitment (Supplementary Fig. 6a–l). In agreement with this notion, FACS analysis revealed that ~20% of the total GFP^{AT+} cells are doubly labeled with Dpp4 and Pdgfrα (Supplementary Fig. 6m–p). Finally, we performed qPCR analysis on FACS sorted GFP-negative and GFP^{AT}-positive cells for lineage markers. Indeed, we observed enrichment of adipose lineage genes within the GFP^{AT+} cellular pool compared to the GFP-negative cells (Supplementary Fig. 6q). Thus, the AdipoTrak genetic tool marks the prospective adipose progenitor lineage.

While *Cxcr4* mRNA expression remained comparable between male and female GFP^{AT+} cells, the percentage of Pparγ-labeled cells expressing Cxcr4 protein was more abundant in female iWAT and gWAT depots than in males (Fig. 1e–g, and Supplementary Fig. 6r). These results appeared to be independent of GFP^{AT+} number as both male and female WAT depots had comparable AdipoTrak-marked cell populations (Supplementary Fig. 6s). Yet, as previously reported[45], gWAT depots contained more progenitors than iWAT regardless of sex (Supplementary Fig. 6s). Together, *Cxcr4* is expressed throughout the Pparγ-labeled cells isolated from adipose but marks more GFP^{AT+} cells within females.

Cxcr4 directs male WAT development

To assess the involvement of *Cxcr4* in the WAT lineage, we generated a mouse model in which *Cxcr4* was deleted in utero and throughout adipose lineage maturation. To do so, we combined the AdipoTrak system (*Pparγ*-tTA; TRE-H2B-GFP[31]) with the *Cxcr4$^{fl/fl}$* conditional mouse model[53] to generate *Cxcr4*^{AT}KO mice. Further, we combined this model with the TRE-Cre recombinase mouse model to drive the deletion of conditional floxed alleles (Fig. 2a). In the absence of doxycycline, the *Pparγ*-tTA driven TRE-Cre is constitutively active, and Pparγ-marked cells will be labeled with GFP. Immunostaining showed reduced Cxcr4 co-expression within GFP^{AT+} cells isolated from *Cxcr4*^{AT}KO male mice (Supplementary Fig. 7a, b). Gene expression and flow cytometric analysis revealed that Cxcr4 expression was specifically reduced within the GFP^{AT+} labeled cell lineage compared to GFP-negative cells within the WAT (Supplementary Fig. 7c–g). Moreover, *Cxcr4* deletion was restricted to adipose depots (Supplementary Fig. 7h). Phenotypically, we found that Control^{AT} and *Cxcr4*^{AT}KO male mice had similar body weight at two months of age (Fig. 2b). However, using nuclear magnetic resonance body composition analysis, we found a ~25% reduction in body fat composition with an increase in lean mass (Fig. 2c and Supplementary Fig. 7i). Changes in male adiposity appeared to be independent of food intake, which was similar between groups (Fig. 2d). While adiposity was lower in *Cxcr4*^{AT}KO male mice, it did not appear to influence glucose clearance (Fig. 2e). Moreover, several WAT-associated blood parameters, such as insulin, triglycerides, adiponectin, and leptin levels, remained unchanged between control and mutant male mice (Supplementary Fig. 7j–m). Visual inspection and weight of the subcutaneous iWAT from *Cxcr4*^{AT}KO mice appeared slightly less than controls (Fig. 2f, g). However, a preferential reduction in the visceral gWAT depot was apparent (Fig. 2f, g). Non-adipose tissue organ weight remained equivalent between control and mutant male mice (Supplementary Fig. 7n). Hematoxylin and eosin (H&E) staining of mutant iWAT and gWAT sections revealed larger adipocytes, suggesting hypertrophy (Fig. 2h). Consistently, quantification of iWAT and gWAT adipocyte area revealed that *Cxcr4* deletion encouraged adipocyte swelling compared to control adipocytes (Fig. 2i). Although there were changes in adiposity, adipocyte genetic profiles within iWAT and gWAT depots were comparable between Control^{AT} and *Cxcr4*^{AT}KO mice (Fig. 2j). Thus, it appears that, in male mice, *Cxcr4* can impact WAT development but WAT remains functional.

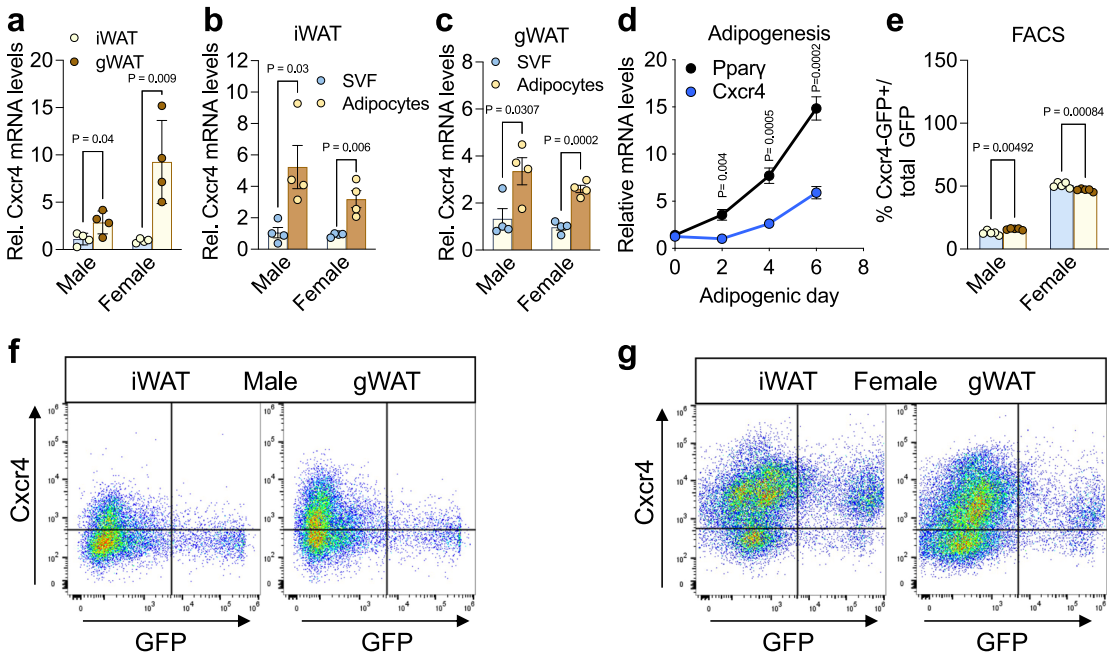

Fig. 1 | Cxcr4 is expressed in mature adipocytes and Pparγ-marked cells. a Cxcr4 mRNA expression within inguinal (iWAT) and perigonadal (gWAT) depots from two-month-old male and female mice ($n = 4$ biological independent mice/group). **b** Cxcr4 mRNA expression within SV cells and floated adipocyte compartments from iWAT (**b**) and gWAT (**c**) depots from two-month-old male and female mice ($n = 4$ biological independent mice/group). **d** Lin-negative SV cells were isolated from iWAT depots and induced with adipogenic media. mRNA expression of Cxcr4 and Pparγ throughout in vitro adipogenesis at denoted days ($n = 4$ biological independent mice/group). **e** Flow cytometric analysis of Cxcr4 and GFP^{AT+} overlap from iWAT and gWAT depots from two-month-old female and male Control^{AT} ($n = 5$ biologically independent mice/group). Representative flow cytometric plots of GFP^{AT+} and Cxcr4 overlap within Control^{AT} (P60) female (**f**) and male (**g**) iWAT and gWAT depots ($n = 5$ biological independent mice/group). Data are means with individual data points ±S.E.M. Statistical significance was determined using unpaired two-tailed Student's *t* test (**a**–**e**).

https://doi.org/10.1038/s41467-024-50985-8

Cxcr4 is necessary for female WAT development

While evaluating *Cxcr4*^{AT}KO male mice, we noticed female *Cxcr4*^{AT}KO littermates appeared lean. Even though, at P60, body weight was similar between Control^{AT} and *Cxcr4*^{AT}KO female mice, body composition analysis revealed a ~50% reduction in adiposity in female mutant mice but with an increase in lean mass (Fig. 3a, b and Supplementary

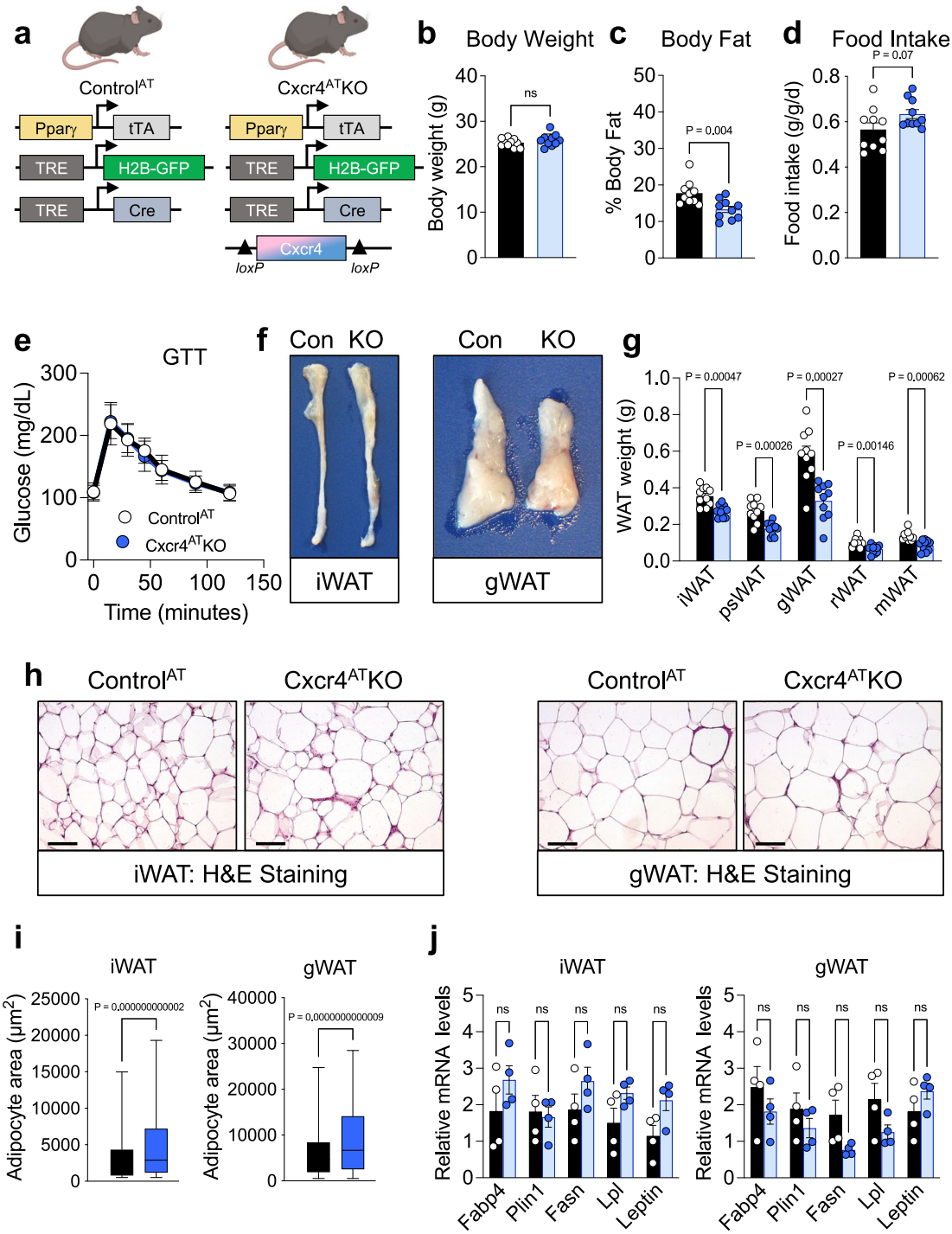

Fig. 2 | Cxcr4 contributes to male WAT development. a Genetic design: allelic combination used to create AdipoTrak-control (Control^{AT}) and AdipoTrak-Cxcr4-KO (Cxcr4^{AT}KO). **b**–**e** Two-month-old (P60) Control^{AT} and Cxcr4^{AT}KO male mice were phenotypically evaluated for: body weight (**b**), body fat content (**c**), food intake (**d**), and glucose clearance by GTT (**e**) ($n = 10$ biologically independent mice/group). **f** Representative photographical images of iWAT and gWAT depot from mice described in **b**. **g** WAT depot weights from mice described in **b** ($n = 10$ biologically independent mice/group). **h** Representative images of H&E staining of iWAT and gWAT sections from mice described in **b**. **i** Quantification of iWAT and gWAT adipocyte area from images described in **h** from mice described in **b** ($n = 3$ biologically independent mice/group). **j** Directed qPCR analysis of pan-adipocyte marker gene expression within iWAT and gWAT depots from mice described in **b** ($n = 4$ biologically independent mice/group). Data are means with individual data points ±S.E.M expect (**i**) represented by box and whisker plot with minimum and maximum. In **i**, the lower, central, and upper line in each box represents the first, the second (median), and the third quartile. Statistical significance was determined using unpaired two-tailed Student's *t* test (**b**–**e**, **g**, **i**, and **j**) (ns = not significant). Scale bar = 100 μm. Created with BioRender.com released under a Creative Commons Attribution-NonCommercial-NoDerivs 4.0 International license (https://creativecommons.org/licenses/by-nc-nd/4.0/deed.en).

https://doi.org/10.1038/s41467-024-50985-8

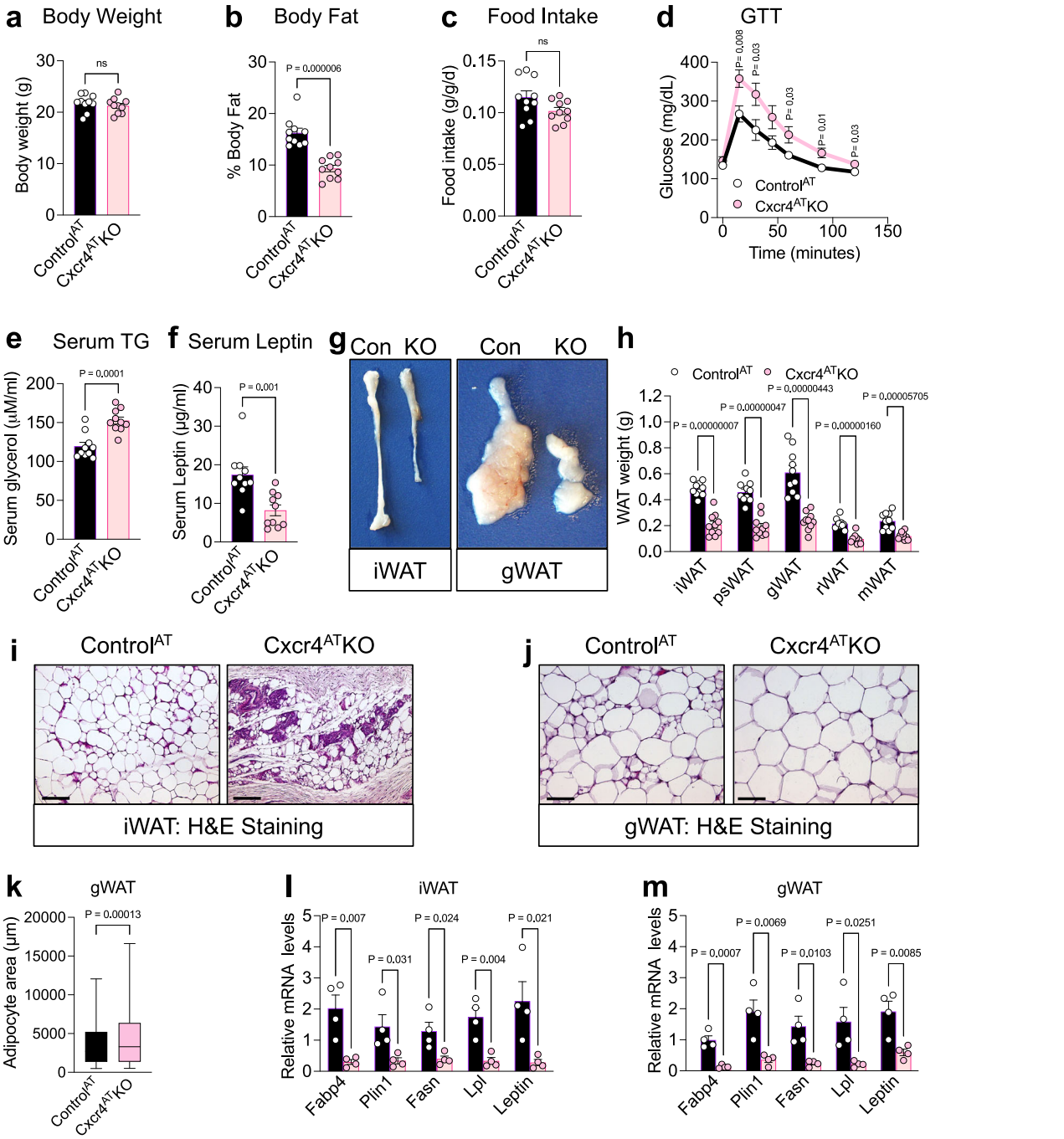

Fig. 3 | Cxcr4 is necessary for female adiposity. Two-month-old (P60) Control^{AT} and Cxcr4^{AT}KO female mice were phenotypically evaluated for: body weight (**a**), body fat content (**b**), food intake (**c**), and glucose clearance by GTT (**d**) ($n = 10$ biologically independent mice). Serum triglyceride (TG) (**e**) and leptin (**f**) levels from mice described in **a** ($n = 10$ biologically independent mice/group). **g** Representative photographical image of iWAT and gWAT depots from mice described in **a**. **h** WAT depot weights from mice described in **a** ($n = 10$ biologically independent mice/group). Representative images of H&E staining of iWAT (**i**) and gWAT (**j**) sections from mice described in **a**. **k** Quantification of gWAT adipocyte area from images described in **j** from mice described in **a** ($n = 3$ biologically independent mice/group). Directed qPCR analysis of pan-adipocyte marker gene expression within iWAT (**l**) and gWAT (**m**) depots from mice described in **a** ($n = 4$ biologically independent mice/group). Data are means with individual data points ±S.E.M expect (**k**) represented by box and whisker plot with minimum and maximum. In **k**, the lower, central, and upper line in each box represents the first, the second (median), and the third quartile. Statistical significance was determined using unpaired two-tailed Student's *t* test (**a**–**f**, **h**, and **k**–**m**) (ns = not significant). Scale bar = 100 µm.

Fig. 8a). Like male mice, changes in adiposity appeared to be independent of food intake (Fig. 3c). *Cxcr4*^{AT}KO female mice also demonstrated augmented glucose responses (Fig. 3d). Yet, fasted serum insulin levels were comparable between control and mutant mice (Supplementary Fig. 8b). On the other hand, blood chemistry analysis revealed a ~25% increase in serum triglycerides levels, suggesting impaired lipid storage (Fig. 3e). The decline in adiposity was associated with a ~50% decrease in circulating adiponectin, a marker of WAT health, and leptin, a marker of WAT size, levels. (Fig. 3f and Supplementary Fig. 8c). Visual inspection and weight revealed that all female mutant WAT depots were significantly reduced (Fig. 3g, h). Examination of non-adipose tissue organs from control and mutants revealed

similar weights (Supplementary Fig. 8d). H&E staining of female mutant iWAT sections revealed disrupted tissue architecture and a paucity of adipocytes (Fig. 3i). Mutant female gWAT had normal WAT architecture, but remnant adipocytes were hypertrophied (Fig. 3j, k). Correspondingly, mRNA analysis of mutant female iWAT and gWAT depots showed reduced adipogenic genes and mature adipocyte markers (Fig. 3l, m). Of note, gene expression and flow cytometric analysis validated Cxcr4 deletion within GFP^{AT+} cells compared to other compartments (Supplementary Fig. 8e–i). Moreover, *Cxcr4* expression was reduced in WATs but was unaffected in non-adipose tissue organs (Supplementary Fig. 8j). Taken together, it appears that *Cxcr4* is critical for WAT development in female mice.

Deleting *Cxcr4* promotes WAT fibrosis and inflammation

Histological staining of *Cxcr4*^{AT}KO WAT sections, notably females, revealed reduced adiposity and distorted microarchitecture, but the most prominent feature was a marked presence in fibrotic tissue within iWAT and gWAT depots (Fig. 3i, j). We performed picrosirius red staining on male and female iWAT and gWAT sections to confirm these observations. Male *Cxcr4*^{AT}KO iWAT tissues appeared slightly more fibrotic than control; however, no fibrotic differences were observed in gWAT depots (Fig. 4a and Supplementary Fig. 9a). In stark contrast, picrosirius red staining of female *Cxcr4*^{AT}KO iWAT specimens showed robust fibrotic tissue replacement with gWAT being less severe (Fig. 4b and Supplementary Fig. 9b). As a next step, we performed directed qPCR on fibrotic genes from male and female control and mutant iWAT and gWAT depots. Indeed, fibrotic markers were upregulated in male and female *Cxcr4*^{AT}KO mutant iWATs compared to controls (Fig. 4c, d). Fibrotic genes were elevated within female *Cxcr4*^{AT}KO gWAT depots but not within mutant male gWAT specimens (Fig. 4c, d). Fibrotic tissue replacement is usually accompanied by tissue inflammation[54]. In agreement, F4/80, a general marker of inflammation[55], immunostaining revealed the presence of more crown-like structures within mutant gWAT depots from female, not male, mutants (Fig. 4e, f and Supplementary Fig. 9c–e). Correspondingly, proinflammatory mRNA analysis only revealed changes in tumor necrosis factor alpha (*Tnfα*) within iWAT and gWAT depots of mutant male mice, which may be attributed to hypertrophy-induced changes in adipokine secretion profiles (Fig. 4g)[56]. However, proinflammation genes were markedly elevated within female *Cxcr4*^{AT}KO WAT depots (Fig. 4h). We validated our immunological studies by analyzing the frequency of macrophages directly by flow cytometry, using CD68 as a marker[57]. The total number of macrophages remained equivalent between male control and mutant WAT depots (Supplementary Fig. 9f). In contrast, the number of Cd68+ macrophages were significantly higher in mutant female WAT depots than in controls (Supplementary Fig. 9g). Dysfunctional WAT fosters ectopic lipid accumulation in other organs such as liver[58]; yet, at P60, *Cxcr4*^{AT}KO mice (male or female) did not present with liver steatosis at this early age (Supplementary Fig. 9h, i). Together, ablating *Cxcr4* within the adipose lineage in female mice reduces adipose tissue growth and promotes fibrotic tissue replacement and inflammatory signals, which promotes metabolic disruption.

Deleting *Cxcr4* alters *Pparγ*-marked cellular dynamics

The lack of an adipocyte phenotype coupled with our flow cytometric analysis and changes in adipose tissue composition in *Cxcr4*^{AT}KO female mice made us hypothesize that *Cxcr4* might induce changes in cellular dynamics of Pparγ-marked cells. Towards this end, we used the TRE-H2B-GFP reporter within the AdipoTrak system to evaluate proliferating and quiescent Pparγ-labeled cells[59]. First, we used whole-mount immunofluorescence to assess GFP^{AT+} presence within the various depots. This cursory observation of male and female iWAT and gWAT depots showed that GFP^{AT+} cells were in the correct anatomical anlagen (Fig. 5a, b). Of note, GFP^{AT+} expression was barely detectable in non-adipose tissues by whole mount fluorescence and flow cytometric analyses (Supplementary Fig. 10a–d). Additionally, FACS analysis did not reveal erroneous expression of GFP^{AT+} cells in other organs in response to *Cxcr4* deletion in either sex (Supplementary Fig. 10e, f). Correspondingly, flow cytometric profiling revealed that *Cxcr4*-deletion did not modify the AdipoTrak lineage confinement, such as labeling hematopoietic, endothelial, and monocyte lineages, consistent with the notion that GFP^{AT+} labeled cells represent adipogenic progenitors in male and female WAT depots (Supplementary Figs. 11a–h and 12a–f).

APCs can reside in various states of adipogenic commitment; therefore, we probed if *Cxcr4* deletion altered the GFP^{AT+} cell population. Using flow cytometric analyses, we found similar total GFP^{AT+} cellular pool sizes within iWAT and gWAT depots between control and mutant male mice (Supplementary Fig. 13a). In opposition, female *Cxcr4*^{AT}KO iWAT and gWAT depots showed an increase (~3–5%) in the GFP^{AT+} cellular pool (Fig. 5c). Yet, *Cxcr4*^{AT}KO-induced changes in the female GFP^{AT+} population were not linked to increased proliferation (Fig. 5d, e). For instance, male flow cytometric profiles revealed analogous 5-bromo-2'-deoxyuridine (BrdU) incorporation between Control^{AT} and *Cxcr4*^{AT}KO labeled cell populations (Supplementary Fig. 13b, c). In contrast, *Cxcr4*^{AT}KO females had diminished iWAT and gWAT GFP^{AT+} cellular BrdU incorporation, suggesting a more quiescent or quasi-differentiation state (Fig. 5d, e). Regardless of sex or *Cxcr4* deletion, we did not observe proliferation changes in non-AdipoTrak cells (Supplementary Fig. 13d, e). Consistent with proliferative status, we observed less p38/MAPK phosphorylation—a downstream target of Cxcr4 signaling—in mutant female Lin-negative SV cells compared to controls but not in males (Supplementary Fig. 13f–i). In agreement with lower BrdU incorporation into female *Cxcr4*^{AT}KO Pparγ-labeled cells, we observed diminution of a population of cells with intense GFP^{AT+} expression (GFP$^{AT\text{-}hi}$) in female iWAT and gWAT depots (Fig. 5f-h). Notably, GFP$^{AT\text{-}hi}$ cells are considered enriched in Pparγ and could be highly proliferative based on H2B-GFP expression[31,59]. Correspondingly, we observed a marked increase in the *Cxcr4*^{AT}KO GFP$^{AT\text{-}low}$ population, suggesting a lineage shift (Fig. 5f–h). However, we did not observe changes in male control and mutant GFP^{AT+} cells (Supplementary Fig. 13j–m). These data suggest that *Cxcr4* may support and maintain a female population of GFP$^{AT\text{-}hi}$ cells.

The *Cxcr4*-deletion-induced variation in the AdipoTrak-lineage distribution prompted us to test if in vitro adipogenic potential was altered. Towards this end, we isolated Lin-negative iWAT and gWAT SV cells from male and female control and mutant mice and provided adipogenic media (Fig. 5i). Compared to male control adipocyte cultures, *Cxcr4*-deficient SV cells had dampened adipogenic potential (Fig. 5j and Supplementary Fig. 14a, b). Using immunostaining, we confirm that the in vitro adipocytes derived from male *Cxcr4*^{AT}KO cells were Cxcr4 negative (Supplementary Fig. 14c). Conversely, female *Cxcr4*-deficient SV cells were unable to generate lipid-laden adipocytes (Fig. 5k and Supplementary Fig. 14d, e). Taken together, the loss of *Cxcr4*, specifically in female mice, diminishes the AdipoTrak-lineage expansion capacity, which may influence their adipogenic potential.

HFD cannot restore adiposity in *Cxcr4* ablated female mice

To probe if *Cxcr4*^{AT}KO WATs can be provoked to produce adipocytes, we challenged Control^{AT} and *Cxcr4*^{AT}KO mice (male and female) with a high-fat diet (HFD) for 12 weeks[60] (Fig. 6a and Supplementary Fig. 15a). *Cxcr4*^{AT}KO male mice phenotypically and molecularly mirrored Control^{AT} mice on HFD. That is, male controls and mutants had similar body weight, adiposity, glucose clearance, WAT histology, and liver steatosis development (Supplementary Fig. 15b–i). Of note, only mutant iWAT depots remained significantly smaller than controls (Supplementary Fig. 15e). Moreover, we did not detect changes in adipocyte size, fibrotic tissue replacement, or inflammatory responses between male control and mutant mice (Supplementary Fig. 15g–s). As

https://doi.org/10.1038/s41467-024-50985-8

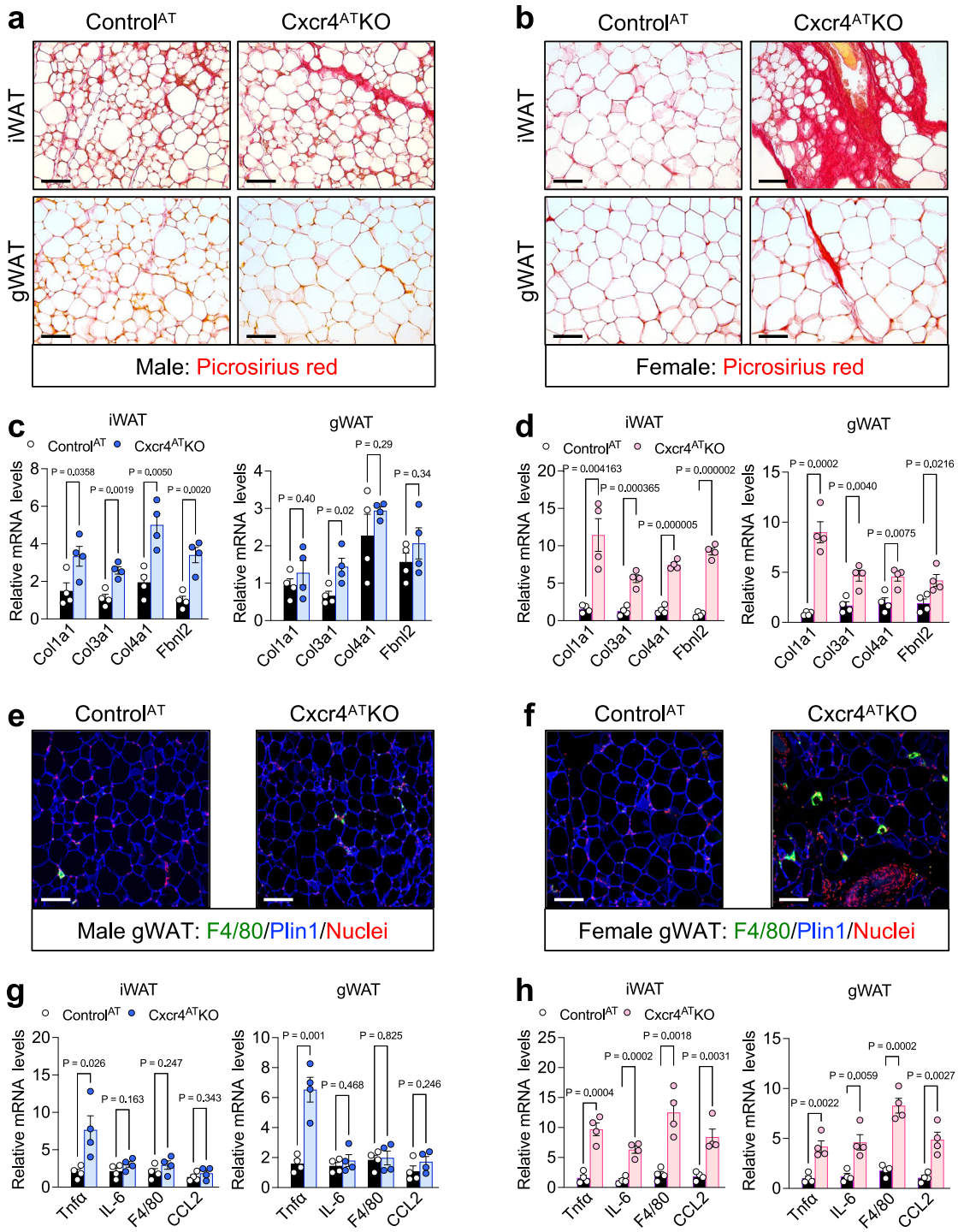

Fig. 4 | Deleting Cxcr4 remodels female WAT. Representative images of picrosirius red staining of iWAT and gWAT sections from two-month-old Control^{AT} and Cxcr4^{AT}KO male (**a**) and female (**b**). Directed qPCR analysis of fibrotic gene expression within Control^{AT} and Cxcr4^{AT}KO male (**c**) and female (**d**) iWAT and gWAT depots ($n = 4$ biologically independent mice/group). Representative F4/80 immunostaining images of gWAT sections from Control^{AT} and Cxcr4^{AT}KO male (**e**) and female (**f**) mice. Directed qPCR analysis of fibrotic gene expression from Control^{AT} and Cxcr4^{AT}KO male (**g**) and female (**h**) iWAT and gWAT depots ($n = 4$ biologically independent mice/group). Data are means with individual data points ±S.E.M. Statistical significance was determined using unpaired two-tailed Student's *t* test (**c**, **d**, **g**, and **h**). Scale bar = 100 μm.

expected, female Control^{AT} mice fed a HFD gained body weight, increased adiposity, and developed glucose intolerance (Fig. 6b–f). In stark contrast, female *Cxcr4*^{AT}KO mice remained lipodystrophic but had impaired glucose clearance like controls (Fig. 6b–f). Histologically, mutant female iWAT sections continued to show a paucity of adipocytes, whereas mutant gWAT adipocytes remained hypertrophied (Fig. 6g, j). Moreover, picrosirius red staining and F4/80 immunostaining showed continued fibrosis and inflammation in iWAT and gWAT depots (Fig. 6h–l). Consistently, mRNA analysis showed reduced adipocyte markers and increased fibrotic and inflammatory genes within *Cxcr4*^{AT}KO female WAT depots (Fig. 6m–o and Supplementary Fig. 16a–c). Corresponding with dysfunctional WAT, we observed a

https://doi.org/10.1038/s41467-024-50985-8

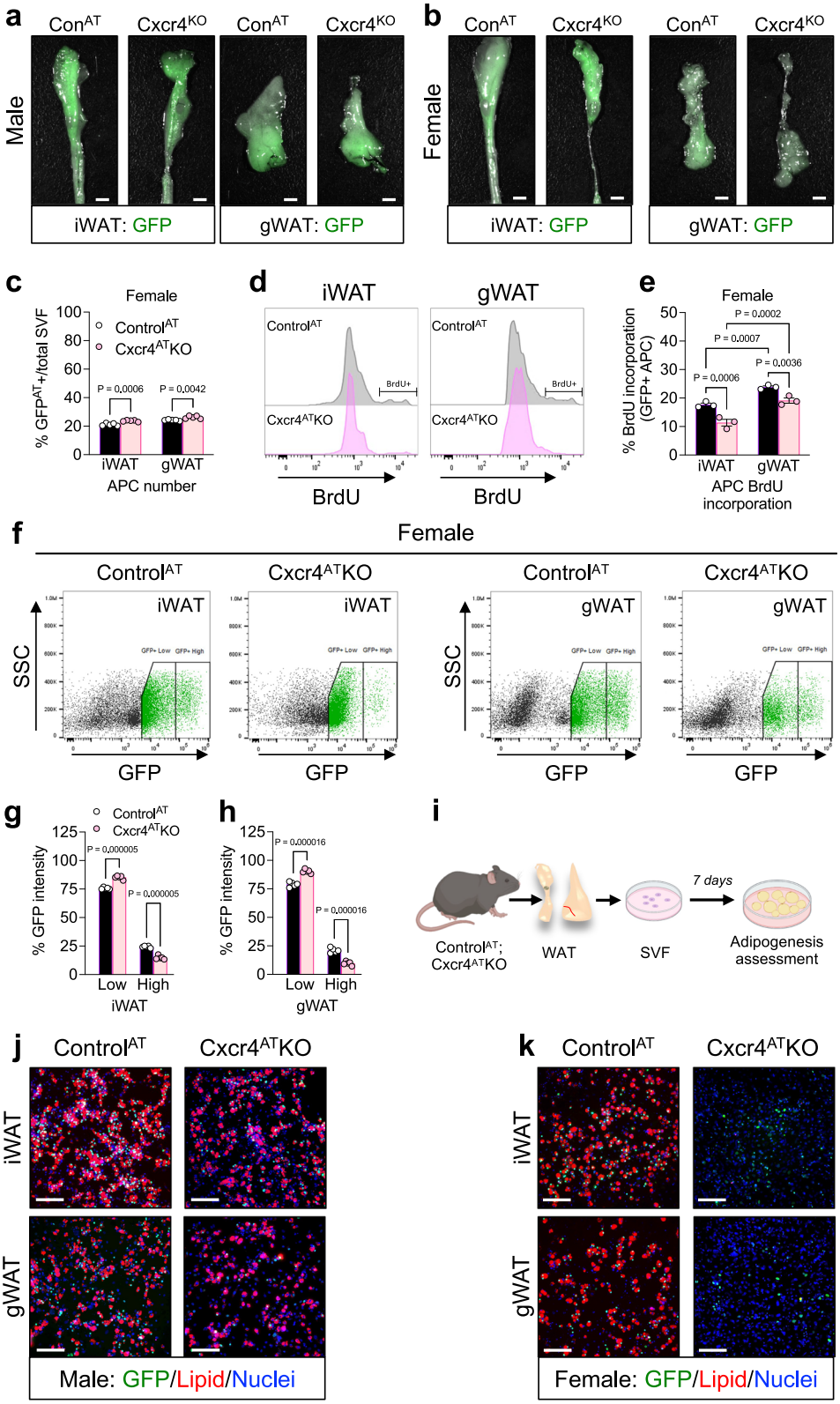

~50% increase in liver weight accompanied by hepatic steatosis in *Cxcr4*^{AT}KO females (Supplementary Fig. 16d, e). Overall, these data suggest that Cxcr4 signaling is critical for female fat mass development but is primarily dispensable for male fat biology.

Cxcr4 deficiency enhances *ERα* expression and activity

Our *Cxcr4*^{AT}KO phenotypical analysis revealed sex-dependent changes in adiposity. Estrogen bioavailability is known to regulate body fat distribution and accumulation. However, these effects depend on estradiol's concentration and WAT depot site, where it can suppress adipogenic potential, prevent lipid storage, or promote lipolysis[6,18]. Thus, we hypothesized that altering Cxcr4 activity may led to a disruption in estrogen signaling. Indeed, we found that the mRNA expression level of estrogen receptor alpha (*ERα*) was elevated in iWAT and gWAT depots of *Cxcr4*^{AT}KO female mice (Fig. 7a). Moreover, immunoblotting showed that ERα protein was upregulated in female

Fig. 5 | Cxcr4 modifies the Pparγ-marked cellular lineage. Representative whole-mount immunofluorescent images of GFP^{AT+} from two-month-old Control^{AT} and Cxcr4^{AT}KO male (**a**) and female (**b**) iWAT and gWAT depots. **c** Flow cytometric analysis of the total GFP^{AT+} within iWAT and gWAT depots from two-month-old Control^{AT} and Cxcr4^{AT}KO male and female mice ($n = 5$ biological independent mice/group). **d** Flow cytometric analysis of BrdU incorporation into iWAT and gWAT GFP^{AT+} cells from two-month-old Control^{AT} and Cxcr4^{AT}KO male and female mice ($n = 3$ biologically independent mice/group). **e** Quantification of BrdU incorporation into iWAT and gWAT GFP^{AT+} labeled cells from Control^{AT} and Cxcr4^{AT}KO female mice ($n = 3$ biologically independent mice/group). **f** Representative flow cytometric profiles of GFP^{AT+} labeled cells within iWAT and gWAT depots from two-month-old Control^{AT} and Cxcr4^{AT}KO female mice establishing GFP$^{AT\text{-}low}$ and GFP$^{AT\text{-}hi}$ populations. 10^5 was determined as the cutoff between GFP$^{AT\text{-}low}$ and GFP$^{AT\text{-}hi}$ populations. Quantification of GFP$^{AT\text{-}low}$ and GFP$^{AT\text{-}hi}$ cellular populations within iWAT (**g**) and gWAT (**h**) depots from flow histograms described in **f** from two-month-old Control^{AT} and Cxcr4^{AT}KO ($n = 5$ biologically independent mice/group). **i** Experimental design: iWAT and gWAT lin-negative SV cells were isolated from two-month-old Control^{AT} and Cxcr4^{AT}KO female and cultured in adipogenic media ($n = 3$ biologically independent mice/group). Adipogenesis was assayed by lipid staining (LipidTox). Representative images of LipidTox staining of adipogenic cultures from SV cells described in **i** from male (**j**) and female (**k**) Control^{AT} and Cxcr4^{AT}KO mice. Data are means with individual data points ±S.E.M. Statistical significance was determined using unpaired two-tailed Student's *t* test (ns = not significant) (**c**, **g**, and **h**) or two-way ANOVA (**e**). Scale bar = 5 mm (**a**, **b**), and 100 μm (**j**, **k**). Created with BioRender.com released under a Creative Commons Attribution-NonCommercial-NoDerivs 4.0 International license (https://creativecommons.org/licenses/by-nc-nd/4.0/deed.en).

Cxcr4^{AT}KO iWAT depots (Fig. 7b). These findings were validated by ERα immunostaining of cultured Lin-negative SV cells (Fig. 7c and Supplementary Fig. 17a). In agreement, flow cytometric analysis of GFP^{AT+} cells from female control and mutant mice revealed that ERα protein was upregulated in iWAT and gWAT *Cxcr4*^{AT}KO samples (Supplementary Fig. 17b). Congruent with sex-dependent changes, ERα expression was slightly elevated in male mutant GFP^{AT+} cells compared to controls (Supplementary Fig. 17c). These subtle changes in male GFP^{AT+} cells may reflect lower abundance of ER expression within male WAT depots[61].

To dissect the functional responses of *Cxcr4* deletion on ERα activity, we attempted to reproduce the *Cxcr4*^{AT}KO female phenotype on mutant male *Pparγ*-labeled cells. Lin-negative SV cells were isolated from iWAT and gWAT depots from Control^{AT} and *Cxcr4*^{AT}KO male mice. Cells were induced with adipogenic media and administered 17β-estradiol (E2) dose-dependently. In control cultures, we found that E2 inhibited adipogenesis at higher concentrations but not at lower doses, as previously observed[27,62] (Fig. 7d, e and Supplementary Fig. 17d, e). In contrast, all E2 concentrations inhibited male *Cxcr4*^{AT}KO adipogenesis (Fig. 7d, e and Supplementary Fig. 17d, e). As a next step, we sought to verify these findings in vivo by administering estradiol (E2; 4.4 μg/mouse) to Control^{AT} and *Cxcr4*^{AT}KO male mice for ten consecutive days (Supplementary Fig. 17f). After ten days of estrogen therapy, flow cytometry revealed similar total GFP^{AT+} cell numbers and GFP intensity distribution in control mice. (Supplementary Fig. 17g–j). In contrast, E2-treated mutant male mice had an overall increase in the total GFP^{AT+} cells. In addition, we noted that E2 treatment produced a higher percentage of the GFP$^{AT\text{-}Low}$ population, whereas the GFP$^{AT\text{-}Hi}$ population decreased, mirroring *Cxcr4*^{AT}KO female GFP^{AT+} cell dynamics (Supplementary Fig. 17i, j). These data suggest that in the absence of *Cxcr4*, GFP^{AT+} cells appear more sensitive to E2, shifting the lineage and diminishing adipogenic potential.

Blocking ERα activity restores Cxcr4^{AT}KO cellular dynamics

Given that ERα activity can reduce adipogenic potential and *ERα* expression positively correlated with *Cxcr4* deletion, we queried if downregulating *ERα* could restore the adipogenic capacity of *Cxcr4*-deficient AdipoTrak-marked cells. Towards this end, we transfected control and mutant female iWAT Lin-negative SV cells with scramble or *ERα*-siRNA prior to adipogenesis, regardless of *ERα* expression control cells differentiated into mature adipocytes (Supplementary Fig. 18a, b). In contrast, knocking down *ERα* in *Cxcr4*-deficient Lin-negative SV cells reestablished adipogenic potential (Supplementary Fig. 18a, b). We continued to explore if blocking ERα activity by administering the antiestrogen fulvestrant (ICI-182780)[63] could restore in vitro *Cxcr4*-deficient Lin-negative SV cell adipogenesis. In control iWAT cultures, low doses of fulvestrant treatment increased adipogenic potential, whereas higher doses did not appear to impact adipogenesis significantly (Fig. 7f, g). Interestingly, fulvestrant did not appear to impact control gWAT Lin-negative SV cell adipogenesis, regardless of dose. Instead, in a dose-dependent manner, fulvestrant treatment increased the presence of visible lipid+ adipocytes in *Cxcr4*^{AT}KO iWAT and gWAT cultures (Supplementary Fig. 18c, d). Of note, while we observed restored adipocyte-lipid staining, not all adipocyte markers (i.e., leptin) were restored (Fig. 7g), highlighting the requirement of *ERα* for adipocyte maturation in *Cxcr4* AdipoTrak-marked cells but the possibility of other mechanisms.

To investigate if fulvestrant could restore the AdipoTrak-labeled cellular pool in *Cxcr4*^{AT}KO female mice, we administered one dose of fulvestrant (5 mg/Kg) to Control^{AT} and *Cxcr4*^{AT}KO female mice for ten consecutive days (Supplementary Fig. 18e). Regardless of genotype, fulvestrant lowered the total GFP^{AT+} number (Supplementary Fig. 18f, g), suggesting that ERα signaling may be critical for maintaining the Pparγ-marked lineage. We further quantified the relative proportion of GFP^{AT+} cells after fulvestrant treatment. Interestingly, in both control and mutant conditions, fulvestrant decreased the GFP$^{AT\text{-}Low}$ population but increased the GFP$^{AT\text{-}hi}$ population in iWAT and gWAT depots (Supplementary Fig. 18h, i). Although fulvestrant remodeled the GFP^{AT+} population in both Control^{AT} and *Cxcr4*^{AT}KO groups, the effect was greater in mutant mice (Supplementary Fig. 18h, i). Thus, ER activity appears to regulate the AdipoTrak-marked cellular pool and may act as an adipogenic brake without *Cxcr4*.

Estrogen removal restores fat mass in *Cxcr4*^{AT}KO mice

The data suggest that the loss of *Cxcr4* potentially enhances *ERα* expression and activity to block adipogenesis in female mice. Therefore, we hypothesized that estrogen removal might restore in vivo adipogenic potential in adult *Cxcr4*^{AT}KO female mice. Towards this end, we performed sham surgery or ovariectomies (OVX) on sexually mature two-month-old Control^{AT} and *Cxcr4*^{AT}KO female mice (Fig. 8a). In response to ovariectomy, both control and mutant mice equally and rapidly gained weight (Fig. 8b). Ovariectomized Control^{AT} mice demonstrated a robust expansion and accumulation of visceral WAT[64,65] (Fig. 8c–e). Shockingly, ovariectomized *Cxcr4*^{AT}KO also showed a dramatic increase and expansion of visceral WAT, with gWAT significantly expanding more than controls (Fig. 8c–e). Consistent with visceral WAT expansion in *Cxcr4*^{AT}KO mice, serum leptin levels were elevated and were associated with more gWAT leptin mRNA expression (Fig. 8f, g). Interestingly, *Cxcr4*^{AT}KO iWAT depots resisted expansion and remained significantly smaller, devoid of adipocytes, fibrotic, and inflamed (Fig. 8d and Supplementary Fig. 19a–e). Histological examination of gWAT sections from ovariectomized Control^{AT} revealed an increase in adipocyte area compared to sham, as expected (Fig. 8h and Supplementary Fig. 19f, g). Yet, adipocyte area quantification of ovariectomized *Cxcr4*^{AT}KO gWAT adipocytes revealed the appearance of smaller adipocytes compared to sham mutants, resembling Control^{AT} sham (Fig. 8h and Supplementary Fig. 19f, g). Because gWAT adipocytes were smaller in ovariectomized *Cxcr4*^{AT}KO female mice, we hypothesized these might be newly generated adipocytes. To test this, we continuously administered BrdU to

https://doi.org/10.1038/s41467-024-50985-8

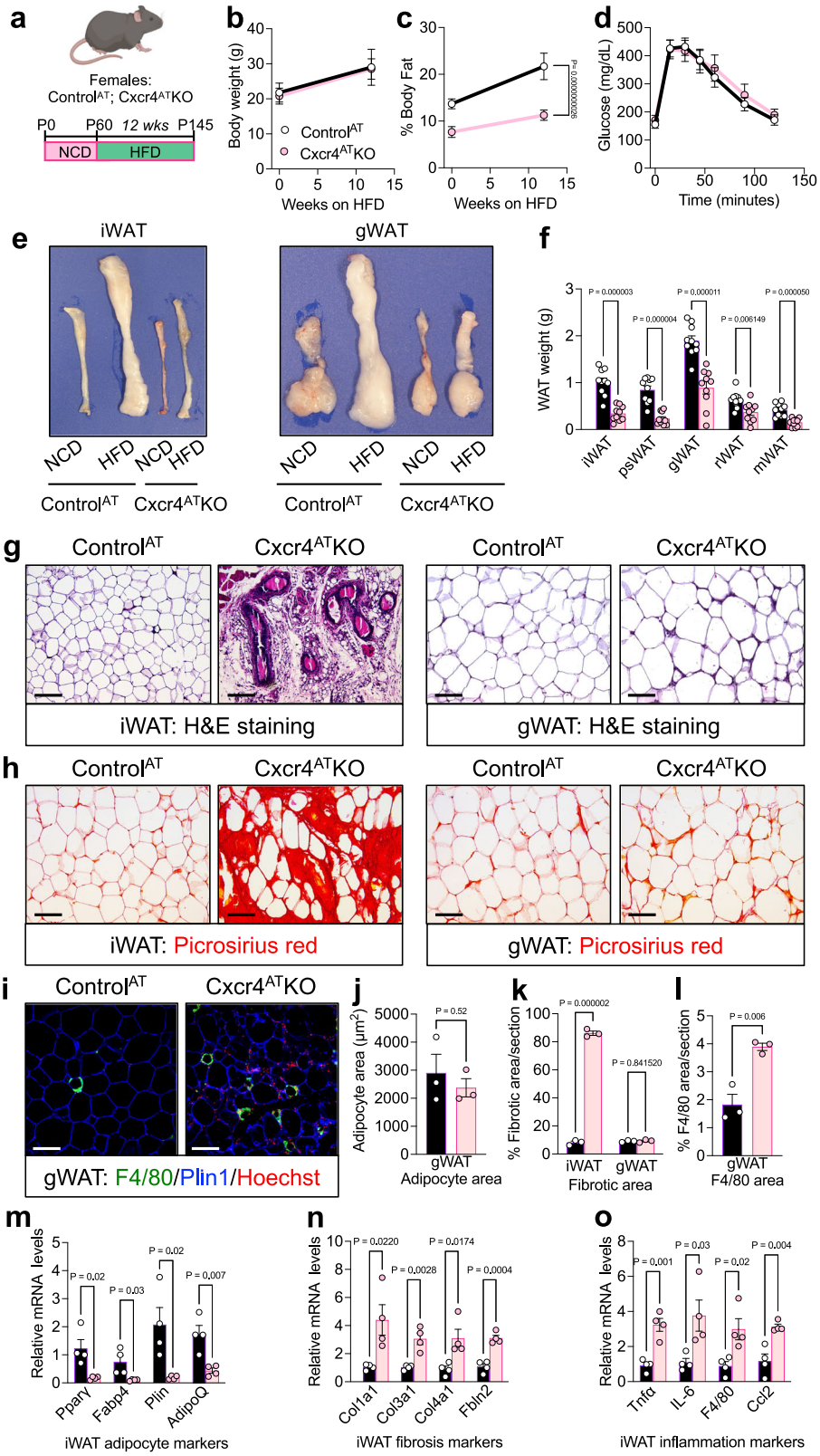

ovariectomized control and mutant mice for 30 days, a suggestive indicator of adipogenesis (Fig. 8i). BrdU immunostaining of gWAT sections from ovariectomized control and mutant mice revealed a three-fold increase in BrdU incorporation into *Cxcr4*^{AT}KO gWAT adipocyte nuclei compared to controls, suggesting progenitor to adipocyte generation in the absence of estradiol (Fig. 8j, k).

Given the appearance of newly generated adipocytes, we explored if estrogen removal restored gWAT homeostasis in *Cxcr4*^{AT}KO female mice. In agreement with fat formation, ovariectomized *Cxcr4*^{AT}KO gWAT depots showed less fibrotic staining than mutant sham gWAT sections (Fig. 8l, m). In concert with restored adiposity and WAT homeostasis, immunostaining revealed lower

Fig. 6 | Cxcr4^{AT}KO female mice resist HFD-induced WAT expansion. Experimental design: two-month-old Control^{AT} and Cxcr4^{AT}KO female mice were maintained on a HFD for 12 weeks (**a**) and evaluated for: body weight growth curve (**b**), body fat content (**c**), and glucose tolerance (**d**) ($n = 10$ biologically independent mice/group). **e** Representative photographical images of iWAT and gWAT depots from Control^{AT} and Cxcr4^{AT}KO maintained on normal chow diet (NCD) or HFD for 12 weeks. **f** WAT depot weights from HFD mice described in **a** ($n = 10$ biologically independent mice/group). Representative images of H&E staining (**g**) and picrosirius red staining (**h**) of iWAT and gWAT sections from Control^{AT} and Cxcr4^{AT}KO female mice described in **a**. **i** Representative images of F4/80 immunostaining of gWAT depots from Control^{AT} and Cxcr4^{AT}KO female mice described in **a**. Quantification of adipocyte size (**j**), fibrotic area (**k**), and F4/80 immunostaining (**l**) from denoted sections from female Control^{AT} and Cxcr4^{AT}KO mice ($n = 3$ biologically independent mice/group). mRNA expression of adipocyte (**m**), fibrotic (**n**), and inflammatory (**o**) markers within iWAT depots from mice described in **a** ($n = 4$ biologically independent mice/group). Data are means with individual data points ±S.E.M. Statistical significance was determined using unpaired two-tailed Student's *t* test (**b**, **c**, **d**, **f**, and **j**–**o**). Scale bar = 100 μm. Created with BioRender.com released under a Creative Commons Attribution-NonCommercial-NoDerivs 4.0 International license (https://creativecommons.org/licenses/by-nc-nd/4.0/deed.en).

F4/80 staining within gWAT depots of ovariectomized mutants compared to sham (Fig. 8n, o). Correspondingly, adipocyte markers were restored, while fibrotic and inflammatory genes were reduced compared to sham mutant levels (Fig. 8g and Supplementary Fig. 19h–l). The changes in *Cxcr4*^{AT}KO visceral WAT driven by estrogen depletion led us to test whether HFD administration could rescue iWAT adiposity under estrogen removal. Towards this end, we fed ovariectomized Control^{AT} and *Cxcr4*^{AT}KO a HFD for four weeks one-week post-surgery (Supplementary Fig. 20a). While body weight remained comparable between control and mutant female mice, we did observe that ovariectomized *Cxcr4*^{AT}KO surpassed Control^{AT} mice in gWAT fat mass accumulation (Supplementary Fig. 20b, c). Notably, under HFD conditions, we observed iWAT depot expansion in *Cxcr4*^{AT}KO after OVX and HFD administration, unlike ovariectomized chow conditions (Supplementary Fig. 20d–f). Picrosirius red staining revealed that mutant iWAT depots contained less fibrosis (Supplementary Fig. 20g, h). Accordingly, we observed less inflammation by F4/80 staining (Supplementary Fig. 20i, j). Correspondingly, gene expression analysis revealed similar levels of adipocyte, fibrotic, and inflammatory markers within iWAT depots of HFD-administered control and mutant ovariectomized mice (Supplementary Fig. 20k–m), suggesting restored and functional fat pads. Because OVX-HFD administration restored *Cxcr4*^{AT}KO iWAT depots, we probed whether new adipogenesis accounted for this expansion by administering BrdU throughout the OVX and HFD time course. Towards this end, we isolated WAT depots, floated adipocytes, isolated adipocyte nuclei, and analyzed BrdU incorporation into GFP^{AT+} adipocyte nuclei by flow cytometry (Supplementary Fig. 21a). Strikingly, we found more BrdU in OVX-HFD *Cxcr4*^{AT}KO adipocyte nuclei than controls (Supplementary Fig. 21b). These data were further confirmed by BrdU immunostaining of iWAT and gWAT sections, suggesting more adipogenesis (Supplementary Fig. 21c–h).

Given that *Cxcr4*-deficiency generated new adipocytes under OVX conditions, we assessed whether OVX could restore Pparγ-marked progenitor dynamics in *Cxcr4*^{AT}KO mice. Four weeks post-surgery (sham and OVX), we FACs evaluated GFP^{AT+} cell number and intensity (Supplementary Fig. 22a). Independent of genotype, estrogen depletion lowered the total GFP^{AT+} cell population within iWAT and gWAT depots (Supplementary Fig. 22b, c). FACS analysis of GFP intensity revealed that OVX decreased GFP$^{AT\text{-}Low}$ cells but increased the GFP$^{AT\text{-}hi}$ cell population in both control and mutant iWAT and gWAT depots (Supplementary Fig. 22d, e). Although OVX altered the GFP^{AT+} cell population in both control and mutants, the effect on *Cxcr4*-deficient *Pparγ*-marked cells was heightened (Supplementary Fig. 22d, e). Taken together, it appears that estrogen depletion can restore fat development in *Cxcr4*^{AT}KO mice and reestablish the *Pparγ* marked lineage within WAT depots.

Cxcr4 antagonism alters murine and human adipogenesis

Our data suggest that *Cxcr4* regulates the adipogenic expansion of a pool of *Pparγ*-marked cells in a sex-dependent manner. This progression appears to be blocked by estradiol and ERα activation, which is augmented in *Cxcr4* deficient cells. In humans, the absence of estradiol triggers subcutaneous fat atrophy and visceral fat expansion; thus, could estradiol therapy be combined with a Cxcr4 antagonist to control adipose-derived stromal cell dynamics and adipogenesis? To examine this possibility, we administered the Cxcr4 antagonist, AMD3100, to male and female Control^{AT} mice for ten consecutive days —to examine immediate responses on *Pparγ*-labeled cells within WAT depots (Fig. 9a and Supplementary Fig. 23a). During this acute phase, AMD3100 treatment did not affect male or female body weight or adiposity (Fig. 9b, c and Supplementary Fig. 23b, c). Additionally, treating male mice with AMD3100 did not affect GFP^{AT+} cell number nor distribution (low, hi) (Supplementary Fig. 23d–h). In female mice, while acute AMD3100 treatment did not produce changes in overall iWAT or gWAT GFP^{AT+} numbers, we did find that AMD3100 increased GFP$^{AT\text{-}Low}$ and decreased GFP$^{AT\text{-}Hi}$ (Fig. 9d–h). Of note, we did not detect changes in GFP^{AT+} status in non-adipose tissue organs in male and female mice treated with AMD3100 (Supplementary Fig. 23i, j). However, in female mice, AMD3100-induced changes in GFP^{AT+} cell distribution and decreased the phosphorylation status of p38/MAPK (Supplementary Fig. 23k, l). These data led us to hypothesize that AMD3100, in combination with estradiol, could mirror our genetic *Cxcr4* modeling and hinder adipogenesis. To test this, we isolated iWAT Lin-negative SV cells from Control^{AT} female and male mice and treated cultures with a vehicle, AMD3100 (1 μm), estradiol (0.01 μm), or the combination (AMD3100 + estradiol) throughout adipogenesis. In male cultures, we found that AMD3100 did not impact adipogenesis; however, estradiol treatment slightly impeded adipocyte formation, as observed in Fig. 7d (Supplementary Fig. 24a, b). However, the combination of AMD3100 and estradiol effectively reduced adipocyte appearance (Supplementary Fig. 24a, b). In female cultures, we found that AMD3100 did not appear to impact adipogenesis, while estradiol slightly enhanced female adipogenesis (Fig. 9i, j and Supplementary Fig. 24c). However, the combination of AMD3100 and estradiol significantly diminished adipocyte generation, paralleling aspects of our genetic model (Fig. 9i, j and Supplementary Fig. 24c). Following these findings, we tested if this effect could be observed in non-obese age-matched female subcutaneous human adipose-derived stromal cells. Administering AMD3100 and estradiol alone slightly blunted overall adipogenesis; however, the combination was more effective at preventing adipocyte development (Fig. 9k, l and Supplementary Fig. 24d). Together, these data suggest that blocking Cxcr4 increases sensitivity to estradiol to alter the Pparγ-labeled cells within WAT and prevent new adipocyte formation.

Discussion

Adipose tissues regulate various biological and metabolic processes such as lifespan, reproduction, glucose and lipid metabolism, and thermogenesis. In turn, changes in nutritional and hormonal cues can alter WAT formation, function, homeostasis, and distribution[66]. Indeed, changes in body fat accumulation and distribution can be quite stark and are major contributors to metabolic disorders, as demonstrated by the prevalence of obesity-associated comorbidities between males and pre- and postmenopausal women. Nevertheless, there is a dearth of knowledge surrounding the molecular mechanisms driving body fat patterning and adipose tissue growth[6]. In this study, we identify *Cxcr4* acting as a rheostat for female adipose tissue-derived

https://doi.org/10.1038/s41467-024-50985-8

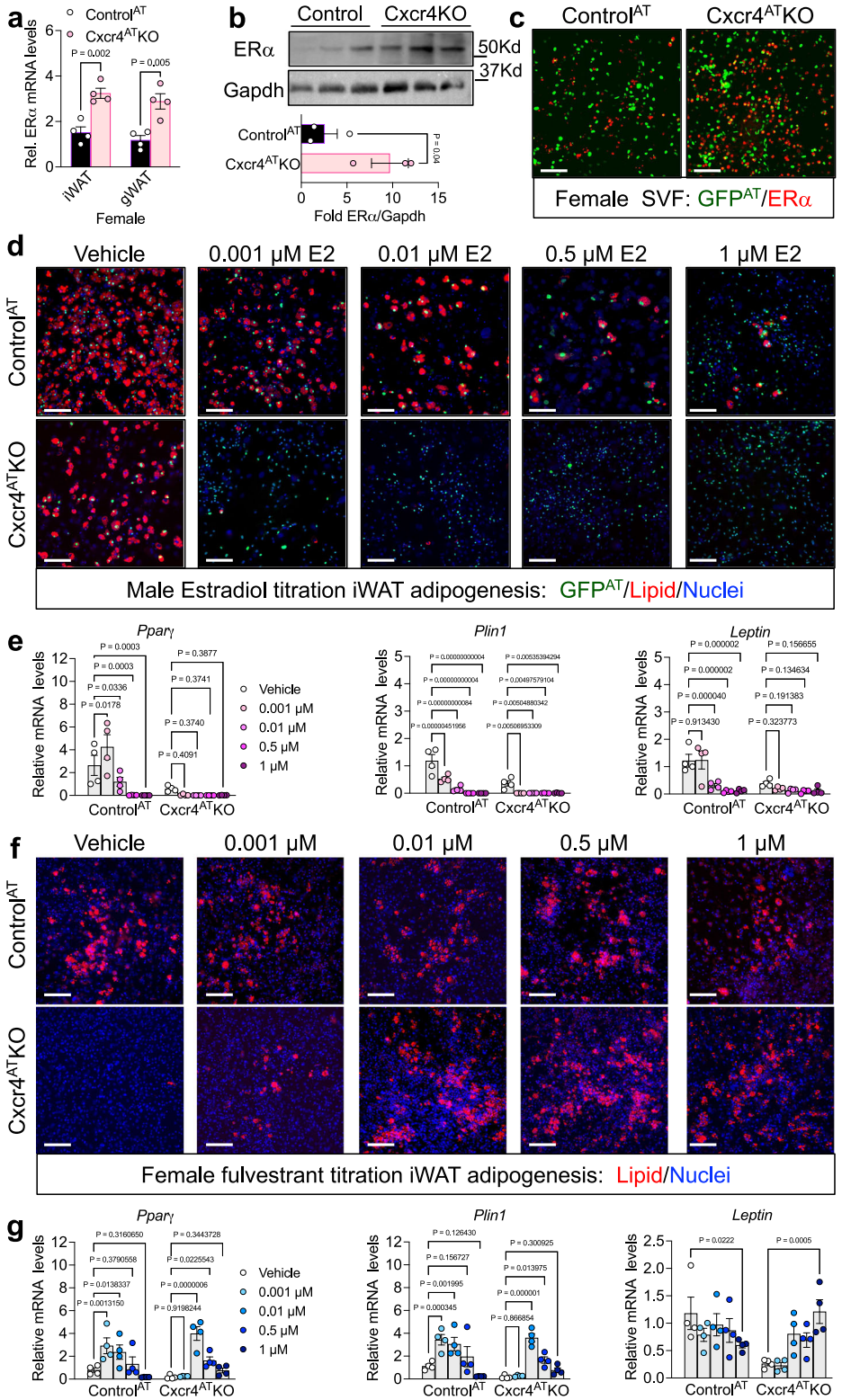

Fig. 7 | Cxcr4^{AT}KO cells are sensitive to estrogen receptor activity. a mRNA expression of ERα within iWAT and gWAT depots from two-month-old Control^{AT} and Cxcr4^{AT}KO female mice ($n = 4$ biologically independent mice/group). **b** Representative immunoblot of ERα within iWAT depots from two-month-old Control^{AT} and Cxcr4^{AT}KO female mice ($n = 3$ biologically independent mice/group). Below: quantification of the ERα immunoblot. **c** Representative ERα immunostaining images of Lin-negative SV cultures from female Control^{AT} and Cxcr4^{AT}KO iWAT depots. **d** Representative images of lipid staining of adipogenic cultures from two-month-old Control^{AT} and Cxcr4^{AT}KO male mice treated with denoted concentrations of 17β-estradiol (E2). **e** mRNA expression of denoted adipocyte markers from adipogenic cultures described in **d** ($n = 4$ biologically independent mice/group). **f** Representative images of lipid staining of adipogenic cultures from two-month-old Control^{AT} and Cxcr4^{AT}KO female mice treated with denoted concentrations of fulvestrant. **g** mRNA expression of denoted adipocyte markers from adipogenic cultures described in **f** ($n = 4$ biologically independent mice/group). Data are means with individual data points ±S.E.M. Statistical significance was determined using unpaired two-tailed Student's *t* test (**a**, **b**) and one-way ANOVA (**e**, **g**). Scale bar = 100 μm.

https://doi.org/10.1038/s41467-024-50985-8

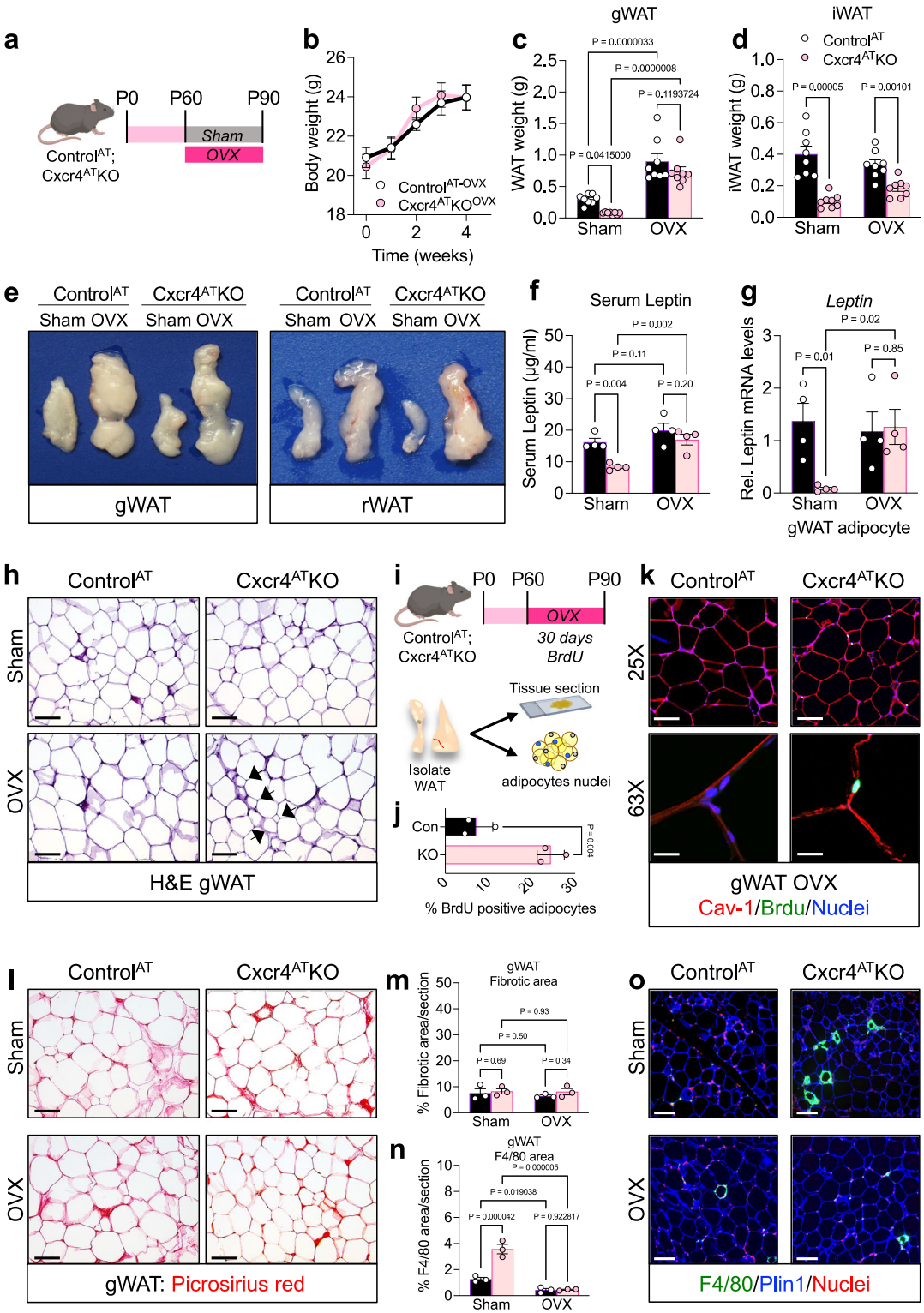

stromal cell function by modulating *ERα* expression and activity to direct adiposity and metabolic responses.

Several lines of evidence suggest that estrogen receptor activity controls the adipose lineage and adiposity in pre- and post-menopausal/ovariectomized states[19,25,26]. Indeed, we find that Cxcr4 suppresses *ERα* expression in a population of proliferating *Ppary*-marked cells, which appears to allow adipogenic progression. Without *Cxcr4*, the *Ppary*-marked cellular pool remains less committed and unable to divide or differentiate in adipocytes. Correspondingly, removing estrogen by OVX or blocking ER activity with antiestrogens, in *Cxcr4*-deficient mice, can restore adipogenic function. Strikingly, alternative methods to provoke adipogenesis, such as HFD, cannot restore adiposity in female *Cxcr4*^{AT}KO mice. On the other hand, male mice respond to HFD signals, yet why might this be the case? We reason that adipogenic signals between male and female mice might differ and require alternative signals and hormones to produce new adipocytes under homeostatic conditions and HFD. Given differences in body fat distribution between females and males, it will be critical to

Fig. 8 | Estrogen removal restores adipogenic potential in Cxcr4^{AT}KO mice. **a**–**d** Experimental design: Sham or ovariectomy (OVX) surgeries were performed on two-month-old Control^{AT} and Cxcr4^{AT}KO female mice (**a**). Subsequently, mice were evaluated 4-wks post-surgery for body weight changes (**b**), and gWAT (**c**), and iWAT (**d**) weight ($n = 8$ biologically independent mice/group). **e** Representative photographical images of visceral WAT depots (gWAT and retroperitoneal WAT (rWAT)) from mice described in **a**. **f** Serum leptin levels from mice described in **a** ($n = 4$ biologically independent mice/group). **g** Leptin mRNA expression within gWAT depots from mice described in **a** ($n = 4$ biologically independent mice/group). **h** Representative images of H&E staining of gWAT sections from mice described in **a**. Black arrows indicate smaller adipocytes. **i** Experimental design: OVX surgeries were performed on two-month-old Control^{AT} and Cxcr4^{AT}KO female mice. Subsequently mice were administered BrdU drinking water continuously for 30 days. Adipocyte nuclei were evaluated for BrdU incorporation. Quantification (**j**) and representative images (**k**) of BrdU immunostaining of gWAT sections from mice described in **i** ($n = 3$ biologically independent mice/group). Representative images of picrosirius red staining (**l**) and fibrotic quantification (**m**) of gWAT sections from mice described in **a** ($n = 3$ biologically independent mice/group). Quantification (**n**) and representative images (**o**) of F4/80 immunostaining of gWAT sections from mice described in **a** ($n = 3$ biologically independent mice/group). Data are means with individual data points ±S.E.M. Statistical significance was determined using unpaired two-tailed Student's *t* test (**b**, **d**, and **j**) and one-way ANOVA (**c**, **f**, **g**, **m**, and **n**). Scale bar = 100 μm. Created with BioRender.com released under a Creative Commons Attribution-NonCommercial-NoDerivs 4.0 International license (https://creativecommons.org/licenses/by-nc-nd/4.0/deed.en).

elucidate adipose lineage differences regulating sex-dependent adipogenesis. Our data also indicate that estradiol has effects on adipogenesis at different doses, which further depends on the depot of origin, sex, and species. Accordingly, it will be crucial to determine the dose of estradiol that coordinates adipose tissue-derived stromal cell lineage dynamics but also affects adipogenesis.

Cxcr4 signaling is associated with sex-dependent biological regulation[67]. For example, Cxcr4 communicates with ERα/β to foster breast cancer progression[67]. Interestingly, this circuit requires Cxcr4 signaling to enhance ER transcriptional activation, which then upregulates the Cxcr4 ligand, *Cxcl12*, creating a feedforward loop. Notably, Cxcr4 signaling via p38/MAPK enhances the phosphorylation of ER to boost transcriptional activity in breast cancer cells[67]. While our studies suggest that Cxcr4 antagonizes ER activity, we do find that p38/MAPK phosphorylation is reduced in the absence of *Cxcr4*. Yet, how this pathway controls ERα activity or expression remains unrealized. The inverse differences between WAT (negative feedback) and breast cancer (positive feedback) in Cxcr4-ER communication could be ascribed to steady-state physiology compared to the oncogenic state[67]. It is possible and remains to be established whether Cxcr4-ER crosstalk becomes disrupted under the obesogenic state, influencing WAT growth and metabolic disease occurrence in a sex-dependent manner. Notably, *Cxcr4* mRNA expression has been shown to be upregulated within WAT depots of obese mice, implicating a potential involvement of this pathway.

The regulation of adipose tissue development and homeostasis by chemokine receptors represents a promising area of research. Although the role of chemokine receptor signaling in mediating inflammatory responses in obesity is well-characterized, the mechanisms by which these receptors influence adipocyte physiology and adipogenic potential have not been fully explored[68–70]. Recent studies have identified the chemokine receptor Cxcr2 as a key regulator of adiposity[46]. Specifically, Cxcr2-KO mice display reduced total adiposity and diminished adipogenic capacity in vitro. Intriguingly, Cxcr2-KO mice exhibit a pronounced sex-dependent adipose tissue phenotype, with female Cxcr2-KO mice having significantly less adipose tissue compared to males[46]. Our data align with these observations, suggesting that Cxcr4 similarly regulates adipose tissue development in a sex-specific manner, predominantly affecting females. However, the precise molecular mechanisms underlying Cxcr2 and Cxcr4 signaling pathways remain to be clarified[46]. Further investigation into other chemokine receptors may also reveal sex-dependent differences in adipose tissue regulation and related metabolic disorders.

Cxcr4 appears to regulate adult adipose tissue-derived stromal cell proliferation and may be involved in a population of adipogenic progenitors that highly express the *Pparγ* driven-tTA TRE-H2B-GFP. Interestingly, *Cxcr4*^{AT}KO cells do not appear to egress from the tissue; instead, *Cxcr4*^{AT}KO cell proliferation is diminished[71]. Intriguingly, our studies reveal that the *Pparγ*-labeled population appears dynamic and resides in different proliferative states. These findings raise many unanswered questions about the AdipoTrak labeled adipose lineage, such as their functionality, how they are regulated, overlap with other lineage markers, and their overall contribution to the lineage trajectory and adipogenesis. Moreover, *Cxcr4* appears to control *Pparγ*-labeled cell dynamics and *ERα* expression; thus, do *Cxcr4*+ cells represent more "stem-like" progenitors and give rise to a more committed adipogenic population or vice versa? A caveat of our study is we only evaluate *Cxcr4* expression and regulation in *Pparγ* marked cells, which has been shown by single cell datasets to be expressed within committed progenitor[72]. However, the AdipoTrak system relies on lineage labeling and not only active Pparγ marking, suggesting cells can be lineage-positive but Pparγ negative[40,41,52]. Nonetheless, additional examination of *Pparγ*-marked cells, using AdipoTrak, will help define *Pparγ* expression and adipose lineage trajectory. Together, continued understanding and "omics" technology, such as transcriptomics, intersectional genetics, and fate mapping methodologies will aid in defining the adipose lineage in a sex-dependent manner.

Hormone or estrogen replacement therapy (HRT) is a commonly prescribed treatment to counteract the physiological changes of menopause[17,73]. However, prescribing estrogen replacement therapy may be contraindicated due to breast cancer susceptibility and hormone tolerance and dosing[74]. Our in vitro data suggest that blocking Cxcr4 activity could be combined with HRT for those who can receive estrogen. This combined therapy could effectively block postmenopausal changes in body fat distribution and accumulation and protect against metabolic disease. Additionally, because Cxcr4 inhibition enhances ER activation, potentially lowering the dose of estradiol may be advised, making estradiol more efficacious. Still, further studies and proof of principle models are required to understand the systemic effects of Cxcr4 inhibition, efficacious dosing, and combinatorial estrogen therapy. Nevertheless, our data indicate that *Cxcr4* is critical for maintaining female WAT homeostasis by modulating *ERα* expression in adipose tissue-derived stromal cells marked by *Pparγ*. Additionally, we provide evidence of a Cxcr4-ER communication network coordinating adipose tissue-derived stromal cells function and lineage trajectory of *Pparγ* marked cells to control body fat distribution in a sex-dependent manner.

Methods

Mouse models

All animal experiments were performed according to procedures approved by the Cornell University Institutional Animal Care and Use Committee under the auspices of protocol number 2017-0063. AdipoTrak was previously[31] created using the following genetic models: *Pparγ* -tTA (strain #024755 Jackson Laboratories[31]), TRE-Cre (tetO-cre; strain #006234[75]; Jackson Laboratories) and TRE-H2B-GFP (generously provided by Dr. Tudorita Tumbar[59]). Offspring were intercrossed for six generations prior to experimentation and were maintained on mixed C57BL/6J-129SV background. AdipoTrak mice were combined with the *Cxcr4*$^{fl/fl}$ conditional mouse model purchased from Jackson laboratories (strain #008767[53]). Adiponectin-Cre mice were purchased from Jackson laboratories (strain #028020[50]) Heterozygous mice

https://doi.org/10.1038/s41467-024-50985-8

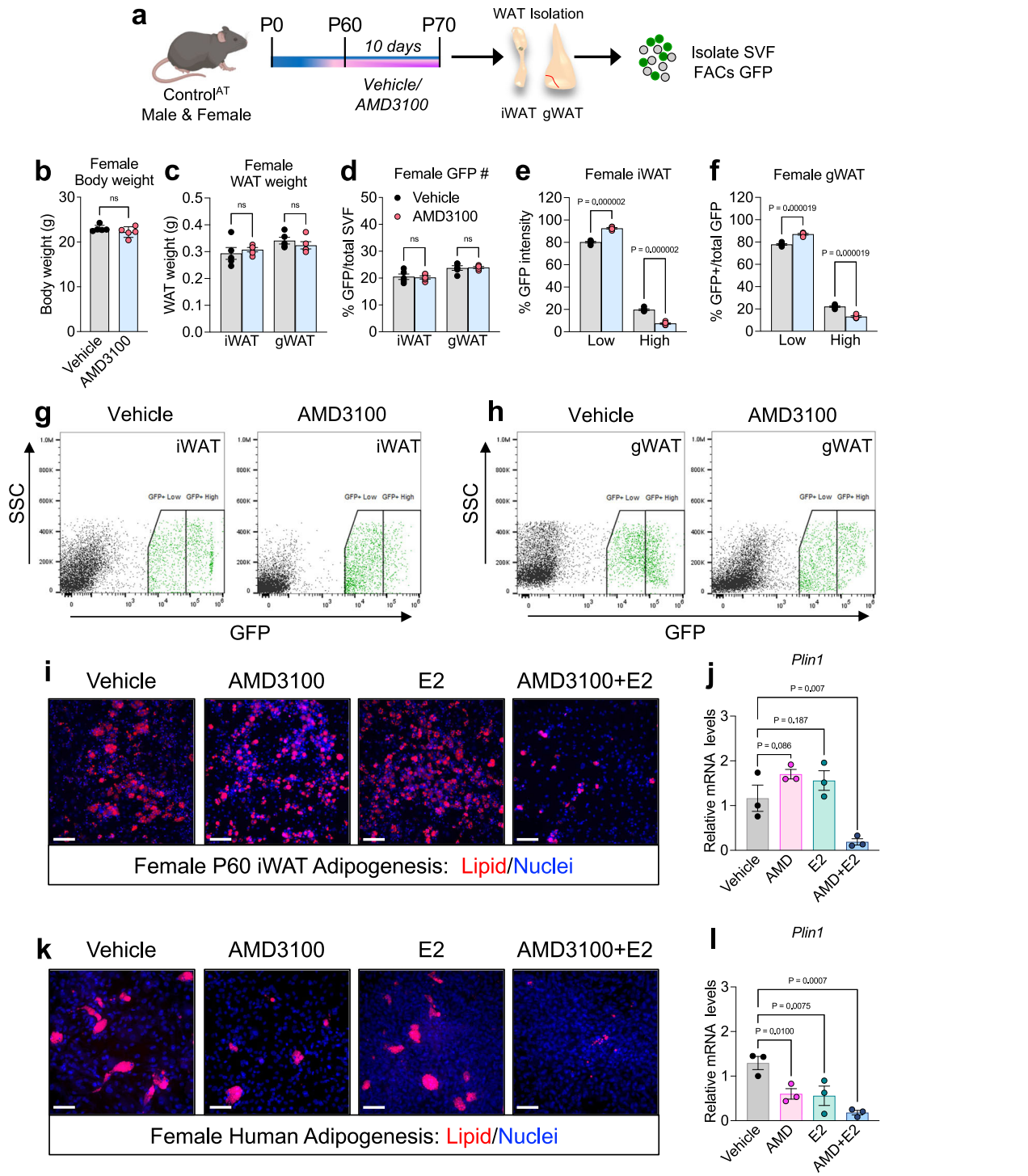

Fig. 9 | Cxcr4 antagonism alters murine and human adipogenesis. **a** Experimental design: Two-month-old male and female Control^{AT} mice were administered one dose of vehicle or AMD3100 (5 mg/Kg) for ten consecutive days. Body (**b**) and WAT (**c**) weight were evaluated from mice described in **a** ($n = 5$ biologically independent mice/group). **d** Quantification of flow cytometric analysis of the total GFP^{AT+} cellular pool within iWAT and gWAT from mice described in **a** ($n = 5$ biologically independent mice/group). Quantification of GFP$^{AT\text{-}low}$ and GFP$^{AT\text{-}hi}$ populations within iWAT (**e**) and gWAT (**f**) depots from flow histograms described in **g**, **h** from vehicle and AMD3100 female mice ($n = 5$ biologically independent mice/group). Representative flow cytometric profiles of GFP$^{AT\text{-}low}$ and GFP$^{AT\text{-}hi}$ cellular populations within iWAT (**g**) and gWAT (**h**) depots from vehicle and AMD3100 female mice. Representative images (**i**) and mRNA expression (**j**) of adipocyte markers of iWAT Lin-negative SV cell adipogenic cultures treated with vehicle (5% DMSO), AMD3100 (1 μM), estradiol (0.01 μM), and AMD3100 + estradiol ($n = 3$ biologically independent mice/group). Representative images of lipid staining (**k**) and mRNA expression (**l**) of adipocyte markers from female human adipose-derived stromal cell adipogenic cultures treated with vehicle, AMD3100, estradiol, and AMD3100 + estradiol ($n = 3$ biologically individual humans). Data are means with individual data points ±S.E.M. Statistical significance was determined using unpaired two-tailed Student's t test (**b**–f) and one-way ANOVA (**j**, **i**). Scale bar = 100 μm. Created with BioRender.com released under a Creative Commons Attribution-NonCommercial-NoDerivs 4.0 International license (https://creativecommons.org/licenses/by-nc-nd/4.0/deed.en).

emanating from this intercross were breed separately to increase the genetic allelic frequency to create control and mutant mice. To maintain inbreeding, every fourth generation, mice were backcrossed to the original/offspring model to create new breeding pairs for control and experimental mice. Mice were maintained on a 14:10-hour light/dark cycle with free access to food and water. All animal experiments were performed on two-month-old mice unless otherwise stated (annotated in figure legends). All animal experiments were performed on 3 or more mice per cohort and performed at least twice.

In vivo pharmacological treatments

Estradiol. Control^{AT} and *Cxcr4*^{AT}KO male mice were administered one dose of estradiol (4.4 μg/mouse; Cayman Chemicals 1006315) for 10 consecutive days by i.p. injection.

Fulvestrant. Control^{AT} and *Cxcr4*^{AT}KO female mice were administered one dose of fulvestrant (5 mg/kg; Sigma Life Sciences I4409) for 10 consecutive days by intraperitoneal (i.p.) injection.

AMD3100. Control^{AT} and *Cxcr4*^{AT}KO male and female mice were administered one dose of AMD3100 (5 mg/kg; Cayman Chemicals 10011332) for 10 consecutive days by i.p. injection.

High-fat diet

Control^{AT} and *Cxcr4*^{AT}KO male and female mice were fed a high fat diet (Research diets; D12492; 60% fat) for 12 weeks. Prior to and at the completion of the diet, body composition and body weight were collected.

Glucose tolerance test

Glucose tolerance tests were performed on mice fasted for 6 hours. Baseline glucose measurements were determined and then mice were i.p. injected with glucose (1.25 g/kg; Sigma G8270, dissolved in sterile water). Tail blood glucose levels were measured at 0 (fasted), 15, 30, 45, 60, 90- and 120-mins post injection with a Bayer Contour glucometer and strips[44].

Food intake

Mice were individually housed with a predetermined (~100 g) amount of food. Food weight was recorded every 24-hour cycle up to five days. Bedding was analyzed for excess food deposits and such mice were excluded from data collection.

Body composition analysis

Body composition was measured using a nuclear magnetic resonance (NMR) Bruker Minispec LF65 benchtop instrument.

BrdU administration

Control^{AT} and *Cxcr4*^{AT}KO male and female mice were administered one dose of BrdU (100 mg/kg; BD Biosciences 51-2354AK) for five consecutive days by i.p. injection. Alternatively, mice were administered constant BrdU via their drinking water (0.75 mg BrdU/mL).

Ovariectomy

Control^{AT} and *Cxcr4*^{AT}KO female mice were anesthetized with 2.5% isoflurane and a small dorsal incision was made over each ovary. The ovarian bursa membrane was cut to expose the ovary. The surrounding ovarian blood vessel and oviduct was sutured and subsequently the ovary was excised. The incision was closed using 6-0 vicryl sutures for the abdominal wall and staples for the skin. The same procedure was then carried out on the other side for the remaining ovary. Staples were removed 7 days post-surgery. Sham surgeries used similar surgical techniques except ovaries remained intact. Analgesics (ketoprofen) for post-surgical pain was administered (once/day for 2-3 days)[76]. Ovariectomies were performed by the Cornell Progressive Assessment of Therapeutics (PATh) facility surgical team.

Blood chemistry

Blood was collected via heart puncture and allowed to coagulate for 2 hours at room temperature (RT). Samples were centrifuged at 3800 × g for 5 minutes. Serum was collected, aliquoted, and frozen. *Insulin ELISA:* To determine serum insulin levels, the mouse Ultrasensitive Insulin ELISA Kit (Ref: 80-INSUMSU-E01) from Alpco was used as per the manufactures protocol. Serum samples were diluted 1:16 prior to measurement. *Adiponectin and Leptin ELISA:* To determine adiponectin and leptin serum levels, the Quantikine ELISA Mouse Adiponectin/Acrp30 (Catalog: MRP30) and Quantikine EISA Mouse/Rat Leptin (Catalog: MOB00B) from R&D systems was used, following the manufactures protocol. Serum was diluted 1:2000 (adiponectin) and 1:200 (leptin) prior to measurement. *Triglyceride Assay:* To determine serum triglyceride levels, the Triglyceride Quantification Colorimetric/Fluorometric Kit from Millipore-Sigma (Sigma-Aldrich Catalog: MAK266) was used, following the manufactures protocol. Serum was diluted 1:25 prior to measurement.

WAT stromal cell isolation

Fat pads were removed and a pair of inguinal or gonadal adipose depots from a single mouse were minced and placed in isolation buffer (0.1 M HEPES, 0.12 M NaCl, 50 mM KCl, 5 mM D-glucose, 1.5% BSA, 1 mM $CaCl_2$) supplemented with collagenase, type I (10,000 units/10 mL) and incubated in a 37 °C incubator with gentle agitation for 1 hour. Serum free Dulbecco's Modified Eagle's Medium Nutrient Mixture F-12 Ham (Sigma, cat. no. D8900 or D6421) (DMEM/F12) media was added to the digested tissue and strained through a 100 (inguinal) or 70 (gonadal)-micron cell straining basket. Samples were spun at 300 × g for 10 minutes to pellet SV cells. The supernatant was removed, and the pellet was resuspended in 10 mLs of erythrocyte lysis buffer (155 mM NH_4Cl, 10 mM $KHCO_3$, 0.1 mM EDTA). After a 5-minute incubation period at RT, growth media (DMEM/F12 supplemented with 10% fetal bovine serum (FBS) was added, mixed, and strained through a 40-micron cell strainer. Samples were then spun at 300 × g for 5 minutes. Supernatant was removed and the cell pellet was resuspended in an antibody cocktail composed of 1 mL MACS buffer (1X PBS, 10% FBS, 2 mM EDTA), 2 μL anti-CD45 and 5 μL anti-CD31 per sample. Samples were then incubated for 20 minutes on ice. Post incubation, 9 mL growth media was added, and samples spun at 300 × g for 5 minutes. The pellet was then resuspended in 2 mL MACS buffer and transferred to 2 mL Eppendorf tubes containing 5 μL prewashed streptavidin beads. Samples were then placed on a rocker for 10 minutes at RT. Samples were then transferred to a magnet for 5 minutes at RT. The supernatant was then collected into 15 mL conical tubes and 5 mL growth media added. Samples were then spun at 300 × g for 5 minutes. The pellet was then resuspended in growth media and cells were plated. After 12 hours, growth media was removed and replenished[77].

Adipogenesis

Isolated cells described above were grown to confluency. Two days post confluency differentiation mix one (DMEM/F12 supplemented with 5% FBS; 10 μg/mL insulin, 1 μM Dexamethasone, 250 μM 3-Isobutyl-1-methylxanthine) was administered for 72 hours. At 72 hours differentiation mix one was removed and differentiation media two (DMEM/F12 supplemented with 10% FBS; 10 μg/mL insulin) was added for the 96 hours. Differentiation was assessed by LipidTox™ staining and mRNA expression of adipogenic markers[78].

Fulvestrant treatment: SVF cells were pretreated with vehicle (5% DMSO) or fulvestrant at the denoted concentrations prior to differentiation. Cells were then induced with adipogenic media as described above in the presence of vehicle and fulvestrant.

Estradiol treatment. SVF cells were pretreated with vehicle (5% DMSO) or estradiol at the denoted concentrations prior to differentiation. Cells were then induced with adipogenic media as described above in the presence of vehicle and estradiol.

AMD3100 treatment. SVF cells were pretreated with vehicle (5% DMSO) or AMD3100 (1 μm) prior to differentiation. Cells were then induced with adipogenic media as described above in the presence of vehicle and AMD3100.

Transfection

SVF cells were isolated as previously described and grown to ~75% confluency prior to transfection in a 24 well plate. Transfection was performed using the Lipofectamine LTX and Plus Reagent kit (Invitrogen 15338-100) according to the manufacturers protocol for 24 well plates with either scramble (Santa Cruz Biotechnology sc-37007) or ER alpha siRNA (Santa Cruz Biotechnology Sc-29306). Cells were then differentiated as previously described post transfection.

Human adipose derived stromal cells and adipogenesis

BMI-matched non-obese human female subcutaneous preadipocyte samples were purchased from Zen-Bio (catalog # SP-F-1-3). Three individual human samples were used for experiments with the following patient details. Sample 1- age: 42, race: Caucasian BMI: 24.69, anatomical location: abdomen; Sample 2- age: 46, race: Caucasian BMI: 24.8, anatomical location: abdomen; Sample 3- age: 52, race: Caucasian BMI: 26.5, anatomical location: abdomen. Human SV cells were grown to confluency in growth media (DMEM/F12 supplemented with 10% FBS). Human SV cells were differentiated using DMEM/F12 supplemented with 5% FBS; 10 μg/mL insulin, 1 μM Dexamethasone, 250 μM 3-Isobutyl-1-methylxanthine for three days. Differentiation mix one was replaced with differentiation mix two (DMEM/F12 supplemented with 10% FBS and 10 μg/ml insulin) for 11 days. Simultaneously, human SV cells were administered vehicle, estradiol (0.01 μm), AMD3100 (1 μm), or the combination of AMD3100/estradiol throughout the differentiation time course, and drugs were replenished every 48 hours.

LipidTox staining

At the end of differentiation, media was aspirated, and adipocytes were fixed with 4% paraformaldehyde for 45 minutes. Adipocytes were washed thrice with 1X TBS with a 5-minute incubation between each wash. Adipocytes were permeabilized using 0.3%TritonX-100 in 1X TBS for 30 minutes. Adipocytes were washed thrice with 1X TBS with a 5-minute incubation between each wash. Adipocytes were incubated with either HSC LipidTox-green or HSC LipidTox-deep red (1:1000 in 1X TBS). Adipocytes were washed twice with 1X TBS with a 3-minute incubation between each wash. Adipocytes were then stained with Hoechst (1 μg/mL in 1XTBS) for 10 minutes. Adipocytes were washed twice with 1X TBS with a 3-minute incubation between each wash. Fluorescent images were collected on a Leica DMi8 inverted microscope system.

Flow cytometry

Adipose SV cells were isolated as described above and resuspended in 1X PBS along with blue-fluorescent reactive dye. Cells were then pelleted (300 × g for 5 minutes) and resuspended in 0.3–0.5 mL of FACS buffer (1X PBS, 5% FBS, 2 mM EDTA) pipetted through 5 mL cell-strainer capped FACS tube (BD Falcon). Cytometry was performed on an BD Biosciences FACS Aria Fusion sorter or a Thermo-Fisher Attune NxT analyzer. Viable cells were gated from the blue-fluorescent reactive dye negative followed by singlet forward and side scatter pattern. The compensation matrix was created for each flow cytometry experiment using the Attune Cytometric Software. Briefly, a negative control, as well as single stained sample for each fluorophore of interest was ran and the data recorded. This was then used to generate the compensation settings for later data analysis. GFP positive and negative cell populations were sorted into 100% FBS for cell culture or RNA analysis. Alternatively, cells were fixed, permeabilized, and stained for BrdU (eFluor 450; 1:200; Invitrogen 48-5071-41), CD68 (AlexaFluor 647; 1:200; Biolegend 137003), Cxcr4/CD184 (APC; 1:400; Biolegend 146507), CD45 (PE-Cy7; 1:200; Invitrogen 25-0451-82), DPP-4/CD26 (PE; 1:100; Biolegend 137803), Pdgfrα/ CD140a (1:200; Invitrogen 14-1401-82), Estrogen Receptor Alpha (1:200; abcam 32063), or Phosphorylated P38/MAPK (1:200 cell signaling 9211) and conjugated to Cy5 donkey anti-rabbit: (Invitrogen A10523, lot 2156245) or Cy5 donkey anti-mouse (Jackson Immunoresearch 715-175-150) fluorphore[41,44].

Histological analysis

Tissues were dissected and immediately placed in 10% formation (neutralized with 1X PBS) for 24 hours. Tissues were processed using an Thermo Scientific™ STP 120 Spin Tissue Processor with the following conditions: Bucket 1: 50% ethanol (45 minutes); Bucket 2: 70% ethanol (45 minutes) Bucket 3: 80% ethanol (45 minutes); Bucket 4 and 5: 95% ethanol (45 minutes); Bucket 6 and 7: 100% ethanol (45 minutes); Bucket 8-10: Xylene; Bucket 11 and 12: paraffin (4 hours). Tissues were embedded into cassettes using a Histostar™ embedding station. Tissues were refrigerated for 24 hours prior to sectioning. 8–12 μm tissue sections were generated using a HM-325 microtome using low profile blades. Sections were placed in a 40 °C water bath and placed on microscope slides. Microscope slides with tissue sections were baked overnight at 55 °C. Slides were rehydrated with xylene (3 mins 3×), 100% reagent alcohol (1 min 2×); 95% reagent alcohol (1 min 2x); water (1 min). Slides were stained in hematoxylin and eosin (H&E) staining for 2:30 minutes and 10 repeated submerges, respectively. Slides were dehydrated in the reverse order as the rehydration steps. Slides were mounted with Cytoseal™ 60. Brightfield images were acquired using a Lecia DMi8 inverted microscope system. Adipocyte area was calculated using ImageJ with the Adiposoft plugin; areas under 50 μm were excluded from control and mutant groups[41,44].

Picrosirius red staining

Slides were de-paraffined and rehydrated under the following conditions: Xylene (3 min 3×), 100% ethanol (1 min 3×), 95% ethanol (1 min 2×), dH2O (30 sec), hematoxylin (3 min). Slides were then washed for 10 minutes under running distilled water. Slides were incubated in 0.1% Sirius Red solution for 45 minutes and washed with 0.5% acidified (glacial acetic acid) water until clear. Subsequently, slides were dehydrated with 100% ethanol (1 min 3×) and xylene (1 min 3×) and mounted with Cytoseal™60 clear mount. Images were captured using a Leica DMi8 inverted microscope system.

Immunostaining

Slides were rehydrated: xylene (3 min 3×), 100% ethanol for (2 min 3×), 95% ethanol for (2 min 2×), running dH2O (1-2 min),1X PBS (10 min). Antigen retrieval was performed using 1X R-Buffer A, made from 10X stock (Electron Microscopy Sciences R-Buffer A, 10X, pH 6; Catalog: 62706-10), and placed into a retriever (EMS Catalog #62706) for 2 hours. Slides were washed in 1X PBS for 15 minutes and permeabilized 0.3% Triton X-100in 1X TBS overnight. Sections were washed with 1X TBS (5 min) and blocked using either 5% donkey serum or goat serum in 1X TBS (30 min) and washed again in 1X TBS (5 min) followed by primary antibody. Primary antibodies against goat anti-Perilipin (1:200; abcam: ab61682), rat anti-F4/80(1:100; RD Systems: MAB5580-SP), rabbit anti-Caveolin-1 (1:400; Cell Signaling: 3238), and rat anti-BrdU (1:350; Abcam: ab6326 clone no. BU1/75 (ICR1)) were used. Sections were washed with 1X TBS for 10 minutes and followed by secondary antibody exposure for 2 hours at room temperature. Secondary antibodies: 488 donkey anti-goat (1:200), Cy5 donkey anti-

rat (1:100; Jackson ImmunoResearch 715-175-150). Washing was repeated with 1X TBS (5 min) and counterstained with Hoechst in 1X TBS (1:1000; H3570; Life Technologies) for 10 minutes or mounted with DAPI Fluoromount-G (Southern Biotech Cat: 0100-20). Images were then obtained with either Leica DMi8 inverted microscope system or Zeiss LSM710 Confocal microscope.

Cell culture staining

Cell culture media was aspirated from cells and were fixed with 4% paraformaldehyde for 45 minutes. Cells were washed thrice with 1X TBS with a 5-minute incubation period between each wash. Cells were permeabilized using 0.3%TritonX-100 in 1X TBS for 30 minutes. Cells were washed thrice with 1X TBS with a 5-minute incubation between each wash. Cells were incubated with 5% donkey serum in 1XTBS for 1 hour. Cells were incubated with primary antibody in 1X TBS with 5% donkey/goat serum either for 1 hour at room temperature (21–23 °C) or overnight at 4 °C. The following primary antibodies were used: goat anti-perilipin (1:100; abcam ab61682); rabbit anti-Cxcr4 (1:1000; ThermoFisher Scientific PA3-305), and estrogen receptor alpha (1:200; abcam ab32063). After incubation with primary antibodies, cells were washed thrice with 1X TBS with a 5-minute incubation between each wash. The following secondaries from Jackson ImmunoResearch were used at 1:200 dilutions: donkey anti-goat; donkey anti-rabbit; and donkey anti-rat. Cells were incubated with secondary antibodies for 2 hours at room temperature. After incubation with secondary antibodies, cells were washed twice with 1X TBS with a 3-minute incubation between each wash. Cells were then stained with Hoechst (1 μg/mL in 1X TBS) for 10 minutes. Cells were washed twice with 1X TBS with a 3-minute incubation between each wash. GFP was directly visualized. Fluorescent images were collected on a Leica DMi8 inverted microscope system.

Immunoblotting

Lineage negative iWAT SV cells were isolated as above, and samples were plated in 10 cm plates. Cultures were then grown, collected, and lysed on ice using 200 μL RIPA lysis buffer containing Pierce protease and phosphatase inhibitor (Thermo Scientific A32959). Lysed samples were then incubated for 30 minutes on ice, spun for 15 minutes at 4 °C, and the supernatant collected. The standard curve and respective protein concentrations for samples were determined and calculated via the protocol provided in the Pierce protein assay kit (Pierce™ BCA Protein Assay - ThermoScientific) and a TECAN infinite F-nano+ spectrophotometer was used to read absorbance. For sample preparation, the calculated volume of 100 μg of protein per sample was mixed at a 1:1 ratio of 2X SDS/DTT, then heated for 10 minutes in a heat block at 100 °C. Prepared samples and protein ladder (Bio-Rad 161-0374) were then loaded into a 10% separating and stacking gel (Bio-Rad 4561034). The gel was placed into a Mini-PROTEAN Tetra Electrophoresis Cell chamber (Bio-Rad 1658004) suspended in 1X running buffer (Bio-Rad 1610744) and ran at 90 V for ~2.5 hours. Protein was then transferred onto an immobilon PSQ PVDF membrane (Millipore ISEQ0005) in 1X transfer buffer (Bio-Rad 1610771) for 1 hour at 100 V on ice. The resulting membrane was removed and washed with 1X TBS-0.1% Tween20 (TBS-T) 3X for 5 minutes on a rocker at room temperature. The membrane was then blocked with 5% BSA in 1X TBS-T for 1 hour at room temperature. Prior to primary antibody addition, the membrane was cut depending on protein of interest molecular weight. Primary antibodies in 5% BSA in 1X TBS-T were added at 4 °C and incubated overnight rocking. The following primary antibodies were used: rabbit anti-phosphorylated p38 (1:1000; Cell Signaling: 4511 S); rabbit anti-GAPDH (1:1000; Cell Signaling: 2118); rabbit anti-vinculin (1:5000; Proteintech: 26510-1-AP); rabbit anti-estrogen receptor alpha (1:500 abcam; ab32063). Membranes were washed again and submerged in secondary antibody for 2 hours at room temperature, rocking (1:5000; ThermoFisher Scientific: donkey anti-rabbit IgG (H + L) Cross-Adsorbed HRP 31458 in 5% Milk 1x TBS-T. Membranes were washed again. To develop, membranes were submerged in a 1:1 solution of SuperSignal™ West Pico PLUS Chemiluminescent Substrate (Thermo-Scientific: 34580) for 3 minutes and developed utilizing a FlourChem E system (biotechne® proteinsimple).

RNA isolation and gene expression analysis

For tissues, 200-300 mg of WAT was placed into Precellys tubes containing ceramic beads and 1 mL of TRIzol (ABI). Tubes were placed in a Precellys 24 homogenizer, and samples were homogenized for 3 pulses at 1400 × g for 30 seconds with a 30 second rest between pulses. For cells, TRIzol was directly added to culture dishes and mechanically disrupted. RNA was extracted using the standard chloroform extraction and isopropanol precipitation method. RNA concentrations and quality were determined using a TECAN infinite F-nano$^+$ spectrophotometer. 1 μg of RNA was converted to cDNA using the high-capacity RNA to cDNA kit (Life Technologies #4368813). Prepared samples were mixed with PowerUp™ SYBR™ Green Master Mix (Life Technologies A25742) and primers (Supplementary Table 1). For human samples and ESR1 measurements, prepared samples were mixed with TaqMan Fast Advanced Master Mix (applied biosystems 4444557) and TaqMan probes as follows: 18 S (FAM 20X Mix Mm04277571_s1), PLIN1 (FAM 20X Mix Hs00160173 m1), FABP4 (FAM 20X Mix Hs01086177 m1), FASN (FAM 20X Mix Hs01005622_m1) Esr1 (FAM 20X Mm00433149 m1). qPCR data was obtained through an Applied Biosystems QuantiStudio™ 3Real-Time PCR system following manufacturer's protocol using the ΔΔ-CT method. Fold values were calculated from these values to compare to the endogenous control Rn18S. All samples were performed in technical quadruplets and 3-4 biological repeats. qPCR primer sequences are available in Supplementary Table 1.

Statistics and reproducibility

Statistical significance was assessed by unpaired Student's *t* test or one- or two-way ANOVA for two-group or multiple group comparisons. Experiments were randomized but were not blinded. Data are means with individual data points presented, when possible, and error bars are expressed as ± S.E.M. A *P*-value of ≤ 0.05 was considered significant in all the experiments. The statistical parameters and the number of mice used per experiment are found in the figure legends. Mouse experiments were performed in biological triplicate with at least three mice per group. Cell culture experiments were collected from three or four technical cultures form three or four biologically independent samples. Flow cytometry experiments were performed on three or four biologically independent mice and repeated at least twice. The flow cytometric analysis software, FlowJo (Version 10; BD Bioscience), was used to analyze cell populations, antibody staining, and generate representative flow plots.

NIH Fiji Image J software was used to quantify percent fluorescent area of total area for F4/80 stains. For Sirius red stains, images were converted to 8-bit black and white images and adjusted with appropriate threshold ranges to highlight fibrotic area. Quantified values represent percent total fibrotic area of total area. For BrdU quantification, 25X images were adjusted for color threshold to count both total amount of BrdU+ nuclei and DAPI+ nuclei. Nuclei residing on the adipocyte membrane were excluded due to reliability. Values represent percent of BrdU+ and DAPI+ nuclei over total DAPI+ nuclei. Three random fields were assessed from at least three biologically independent mice/group for all image quantification. The Fiji ImageJ Adiposoft plugin was used to calculate adipocyte area; areas below 50 microns and adipocytes along edges were omitted due to reliability. Fiji ImageJ software was used to calculate immunoblot densitometry. The Leica Application Suite X Microscope software and Zeiss ZEN Microscopy software were used for image acquisition, z-stack merging, and analyses. All graphs and statistical analysis were performed using

GraphPad Prism 7-9. Excel was used for raw data collection, analysis, and quantification. Experimental designs and schematics were designed using PowerPoint and created with BioRender.com (https://www.biorender.com/).

Reporting summary

Further information on research design is available in the Nature Portfolio Reporting Summary linked to this article.

Data availability

The data that support the findings of this study are available from the corresponding author (DCB) upon request. Source data are provided with this paper.

References

1. Scheja, L. & Heeren, J. The endocrine function of adipose tissues in health and cardiometabolic disease. *Nat. Rev. Endocrinol.* **15**, 507–524 (2019).
2. Berry, D. C., Stenesen, D., Zeve, D. & Graff, J. M. The developmental origins of adipose tissue. *Development* **140**, 3939–3949 (2013).
3. Berry, D. C., Jiang, Y. & Graff, J. M. Emerging Roles of Adipose Progenitor Cells in Tissue Development, Homeostasis, Expansion and Thermogenesis. *Trends Endocrinol. Metab.* **27**, 574–585 (2016).
4. Stefan, N. Causes, consequences, and treatment of metabolically unhealthy fat distribution. *Lancet Diabetes Endocrinol.* **8**, 616–627 (2020).
5. Kivimaki, M. et al. Overweight, obesity, and risk of cardiometabolic multimorbidity: pooled analysis of individual-level data for 120 813 adults from 16 cohort studies from the USA and Europe. *Lancet Public Health* **2**, e277–e285 (2017).
6. Steiner, B. M. & Berry, D. C. The Regulation of Adipose Tissue Health by Estrogens. *Front Endocrinol. (Lausanne)* **13**, 889923 (2022).
7. Geer, E. B. & Shen, W. Gender differences in insulin resistance, body composition, and energy balance. *Gend. Med.* **6**, 60–75 (2009).
8. Menke, A., Casagrande, S., Geiss, L. & Cowie, C. C. Prevalence of and Trends in Diabetes Among Adults in the United States, 1988-2012. *JAMA* **314**, 1021–1029 (2015).
9. Karastergiou, K., Smith, S. R., Greenberg, A. S. & Fried, S. K. Sex differences in human adipose tissues - the biology of pear shape. *Biol. Sex. Differ.* **3**, 13 (2012).
10. Macotela, Y., Boucher, J., Tran, T. T. & Kahn, C. R. Sex and depot differences in adipocyte insulin sensitivity and glucose metabolism. *Diabetes* **58**, 803–812 (2009).
11. Hamer, M., O'Donovan, G., Stensel, D. & Stamatakis, E. Normal-Weight Central Obesity and Risk for Mortality. *Ann. Intern Med.* **166**, 917–918 (2017).
12. Krotkiewski, M., Bjorntorp, P., Sjostrom, L. & Smith, U. Impact of obesity on metabolism in men and women. Importance of regional adipose tissue distribution. *J. Clin. Investig* **72**, 1150–1162 (1983).
13. Byrd-Craven, J. & Geary, D. C. Biological and evolutionary contributions to developmental sex differences. *Reprod. Biomed. Online* **15**, 12–22 (2007).
14. Lee, M. J. & Fried, S. K. Sex-dependent Depot Differences in Adipose Tissue Development and Function; Role of Sex Steroids. *J. Obes. Metab. Syndr.* **26**, 172–180 (2017).
15. Lizcano, F. & Guzman, G. Estrogen Deficiency and the Origin of Obesity during Menopause. *Biomed. Res. Int.* **2014**, 757461 (2014).
16. Carr, M. C. The emergence of the metabolic syndrome with menopause. *J. Clin. Endocrinol. Metab.* **88**, 2404–2411 (2003).
17. Sites, C. K. et al. The effect of hormone replacement therapy on body composition, body fat distribution, and insulin sensitivity in menopausal women: a randomized, double-blind, placebo-controlled trial. *J. Clin. Endocrinol. Metab.* **90**, 2701–2707 (2005).
18. Bracht, J. R. et al. The role of estrogens in the adipose tissue milieu. *Ann. N. Y Acad. Sci.* **1461**, 127–143 (2020).
19. Davis, K. E. et al. The sexually dimorphic role of adipose and adipocyte estrogen receptors in modulating adipose tissue expansion, inflammation, and fibrosis. *Mol. Metab.* **2**, 227–242 (2013).
20. Mauvais-Jarvis, F., Clegg, D. J. & Hevener, A. L. The role of estrogens in control of energy balance and glucose homeostasis. *Endocr. Rev.* **34**, 309–338 (2013).
21. Morselli, E. et al. Impact of estrogens and estrogen receptor-alpha in brain lipid metabolism. *Am. J. Physiol. Endocrinol. Metab.* **315**, E7–E14 (2018).
22. Xu, Y. et al. Distinct hypothalamic neurons mediate estrogenic effects on energy homeostasis and reproduction. *Cell Metab.* **14**, 453–465 (2011).
23. Jensen, E. V. & DeSombre, E. R. Estrogen-receptor interaction. *Science* **182**, 126–134 (1973).
24. Brzozowski, A. M. et al. Molecular basis of agonism and antagonism in the oestrogen receptor. *Nature* **389**, 753–758 (1997).
25. Heine, P. A., Taylor, J. A., Iwamoto, G. A., Lubahn, D. B. & Cooke, P. S. Increased adipose tissue in male and female estrogen receptor-alpha knockout mice. *Proc. Natl Acad. Sci. USA* **97**, 12729–12734 (2000).
26. Lapid, K., Lim, A., Clegg, D. J., Zeve, D. & Graff, J. M. Oestrogen signalling in white adipose progenitor cells inhibits differentiation into brown adipose and smooth muscle cells. *Nat. Commun.* **5**, 5196 (2014).
27. Jeong, S. & Yoon, M. 17beta-Estradiol inhibition of PPARgamma-induced adipogenesis and adipocyte-specific gene expression. *Acta Pharm. Sin.* **32**, 230–238 (2011).
28. Okazaki, R. et al. Estrogen promotes early osteoblast differentiation and inhibits adipocyte differentiation in mouse bone marrow stromal cell lines that express estrogen receptor (ER) alpha or beta. *Endocrinology* **143**, 2349–2356 (2002).
29. Ghaben, A. L. & Scherer, P. E. Adipogenesis and metabolic health. *Nat. Rev. Mol. Cell Biol.* **20**, 242–258 (2019).
30. Hepler, C., Vishvanath, L. & Gupta, R. K. Sorting out adipocyte precursors and their role in physiology and disease. *Genes Dev.* **31**, 127–140 (2017).
31. Tang, W. et al. White fat progenitor cells reside in the adipose vasculature. *Science* **322**, 583–586 (2008).
32. Vishvanath, L. et al. Pdgfrbeta+ Mural Preadipocytes Contribute to Adipocyte Hyperplasia Induced by High-Fat-Diet Feeding and Prolonged Cold Exposure in Adult Mice. *Cell Metab.* **23**, 350–359 (2016).
33. Rodeheffer, M. S., Birsoy, K. & Friedman, J. M. Identification of white adipocyte progenitor cells in vivo. *Cell* **135**, 240–249 (2008).
34. Chawla, A., Schwarz, E. J., Dimaculangan, D. D. & Lazar, M. A. Peroxisome proliferator-activated receptor (PPAR) gamma: adipose-predominant expression and induction early in adipocyte differentiation. *Endocrinology* **135**, 798–800 (1994).
35. Tontonoz, P., Hu, E. & Spiegelman, B. M. Stimulation of adipogenesis in fibroblasts by PPAR gamma 2, a lipid-activated transcription factor. *Cell* **79**, 1147–1156 (1994).
36. Kanda, T. et al. PPARgamma in the endothelium regulates metabolic responses to high-fat diet in mice. *J. Clin. Investig* **119**, 110–124 (2009).
37. Clark, R. B. et al. The nuclear receptor PPAR gamma and immunoregulation: PPAR gamma mediates inhibition of helper T cell responses. *J. Immunol.* **164**, 1364–1371 (2000).
38. Law, R. E. et al. Expression and function of PPARgamma in rat and human vascular smooth muscle cells. *Circulation* **101**, 1311–1318 (2000).
39. Moore, K. J. et al. The role of PPAR-gamma in macrophage differentiation and cholesterol uptake. *Nat. Med.* **7**, 41–47 (2001).
40. Berry, D. C., Jiang, Y. & Graff, J. M. Mouse strains to study cold-inducible beige progenitors and beige adipocyte formation and function. *Nat. Commun.* **7**, 10184 (2016).
41. Jiang, Y., Berry, D. C., Tang, W. & Graff, J. M. Independent stem cell lineages regulate adipose organogenesis and adipose homeostasis. *Cell Rep.* **9**, 1007–1022 (2014).

42. Gupta, R. K. et al. Transcriptional control of preadipocyte determination by Zfp423. *Nature* **464**, 619–623 (2010).
43. Morrison, S. J. & Spradling, A. C. Stem cells and niches: mechanisms that promote stem cell maintenance throughout life. *Cell* **132**, 598–611 (2008).
44. Jiang, Y. et al. A PPARgamma transcriptional cascade directs adipose progenitor cell-niche interaction and niche expansion. *Nat. Commun.* **8**, 15926 (2017).
45. Jeffery, E. et al. The Adipose Tissue Microenvironment Regulates Depot-Specific Adipogenesis in Obesity. *Cell Metab.* **24**, 142–150 (2016).
46. Dyer, D. P. et al. The chemokine receptor CXCR2 contributes to murine adipocyte development. *J. Leukoc. Biol.* **105**, 497–506 (2019).
47. Sakers, A., De Siqueira, M. K., Seale, P. & Villanueva, C. J. Adipose-tissue plasticity in health and disease. *Cell* **185**, 419–446 (2022).
48. Yao, L. et al. Deficiency in adipocyte chemokine receptor CXCR4 exacerbates obesity and compromises thermoregulatory responses of brown adipose tissue in a mouse model of diet-induced obesity. *FASEB J.* **28**, 4534–4550 (2014).
49. Lee, K. Y. et al. Lessons on conditional gene targeting in mouse adipose tissue. *Diabetes* **62**, 864–874 (2013).
50. Eguchi, J. et al. Transcriptional control of adipose lipid handling by IRF4. *Cell Metab.* **13**, 249–259 (2011).
51. Pozzobon, T., Goldoni, G., Viola, A. & Molon, B. CXCR4 signaling in health and disease. *Immunol. Lett.* **177**, 6–15 (2016).
52. Benvie, A. M., Lee, D., Jiang, Y. & Berry, D. C. Platelet-derived growth factor receptor beta is required for embryonic specification and confinement of the adult white adipose lineage. *iScience* **27**, 108682 (2024).
53. Nie, Y. et al. The role of CXCR4 in maintaining peripheral B cell compartments and humoral immunity. *J. Exp. Med.* **200**, 1145–1156 (2004).
54. Muir, L. A. et al. Adipose tissue fibrosis, hypertrophy, and hyperplasia: Correlations with diabetes in human obesity. *Obes. (Silver Spring)* **24**, 597–605 (2016).
55. Austyn, J. M. & Gordon, S. F4/80, a monoclonal antibody directed specifically against the mouse macrophage. *Eur. J. Immunol.* **11**, 805–815 (1981).
56. Arner, E., Ryden, M. & Arner, P. Tumor necrosis factor alpha and regulation of adipose tissue. *N. Engl. J. Med.* **362**, 1151–1153 (2010).
57. Di Gregorio, G. B. et al. Expression of CD68 and macrophage chemoattractant protein-1 genes in human adipose and muscle tissues: association with cytokine expression, insulin resistance, and reduction by pioglitazone. *Diabetes* **54**, 2305–2313 (2005).
58. O'Connell, J. et al. The relationship of omental and subcutaneous adipocyte size to metabolic disease in severe obesity. *PLoS One* **5**, e9997 (2010).
59. Tumbar, T. et al. Defining the epithelial stem cell niche in skin. *Science* **303**, 359–363 (2004).
60. Zeve, D. et al. Wnt signaling activation in adipose progenitors promotes insulin-independent muscle glucose uptake. *Cell Metab.* **15**, 492–504 (2012).
61. Porter, J. W. et al. Age, Sex, and Depot-Specific Differences in Adipose-Tissue Estrogen Receptors in Individuals with Obesity. *Obes. (Silver Spring)* **28**, 1698–1707 (2020).
62. Fatima, L. A. et al. Estradiol stimulates adipogenesis and Slc2a4/GLUT4 expression via ESR1-mediated activation of CEBPA. *Mol. Cell Endocrinol.* **498**, 110447 (2019).
63. Curran, M. & Wiseman, L. Fulvestrant. *Drugs* **61**, 807–813 (2001).
64. Wade, G. N., Gray, J. M. & Bartness, T. J. Gonadal influences on adiposity. *Int J. Obes.* **9**, 83–92 (1985).
65. Babaei, P., Mehdizadeh, R., Ansar, M. M. & Damirchi, A. Effects of ovariectomy and estrogen replacement therapy on visceral adipose tissue and serum adiponectin levels in rats. *Menopause Int.* **16**, 100–104 (2010).
66. Rosen, E. D. & Spiegelman, B. M. What we talk about when we talk about fat. *Cell* **156**, 20–44 (2014).
67. Sauve, K., Lepage, J., Sanchez, M., Heveker, N. & Tremblay, A. Positive feedback activation of estrogen receptors by the CXCL12-CXCR4 pathway. *Cancer Res.* **69**, 5793–5800 (2009).
68. Mraz, M. & Haluzik, M. The role of adipose tissue immune cells in obesity and low-grade inflammation. *J. Endocrinol.* **222**, R113–R127 (2014).
69. Proudfoot, A. E. Chemokine receptors: multifaceted therapeutic targets. *Nat. Rev. Immunol.* **2**, 106–115 (2002).
70. Huber, J. et al. CC chemokine and CC chemokine receptor profiles in visceral and subcutaneous adipose tissue are altered in human obesity. *J. Clin. Endocrinol. Metab.* **93**, 3215–3221 (2008).
71. Girousse, A. et al. The Release of Adipose Stromal Cells from Subcutaneous Adipose Tissue Regulates Ectopic Intramuscular Adipocyte Deposition. *Cell Rep.* **27**, 323–333.e325 (2019).
72. Emont, M. P. et al. A single-cell atlas of human and mouse white adipose tissue. *Nature* **603**, 926–933 (2022).
73. Lamon-Fava, S., Herrington, D. M., Horvath, K. V., Schaefer, E. J. & Asztalos, B. F. Effect of hormone replacement therapy on plasma lipoprotein levels and coronary atherosclerosis progression in postmenopausal women according to type 2 diabetes mellitus status. *Metabolism* **59**, 1794–1800 (2010).
74. Kim, S. M., Kim, S. E., Lee, D. Y. & Choi, D. Serum estradiol level according to dose and formulation of oral estrogens in postmenopausal women. *Sci. Rep.* **11**, 3585 (2021).
75. Perl, A. K., Wert, S. E., Nagy, A., Lobe, C. G. & Whitsett, J. A. Early restriction of peripheral and proximal cell lineages during formation of the lung. *Proc. Natl Acad. Sci. USA* **99**, 10482–10487 (2002).
76. Souza, V. R. et al. Description of Ovariectomy Protocol in Mice. *Methods Mol. Biol.* **1916**, 303–309 (2019).
77. Hausman, D. B., Park, H. J. & Hausman, G. J. Isolation and culture of preadipocytes from rodent white adipose tissue. *Methods Mol. Biol.* **456**, 201–219 (2008).
78. Berry, D. C. & Noy, N. All-trans-retinoic acid represses obesity and insulin resistance by activating both peroxisome proliferation-activated receptor beta/delta and retinoic acid receptor. *Mol. Cell Biol.* **29**, 3286–3296 (2009).

Acknowledgements

The authors thank Dr. Tolunay Beker Aydemir for critically reading the manuscript and helpful suggestions. The authors thank Heather Roman for breeding the mouse colony, technical assistance, and aid in collecting preliminary observations. The authors thank Dr. Jonathan Graff for initial project discussions. The authors thank the Cornell Biotechnology Resources Center Flow Cytometric Core Facility and the Center of Animal Resources and Education for excellent assistance with experimental collection and mouse husbandry, respectively. We thank the Cornell Progressive Assessment of Therapeutics (PATh) facility and Scott Butler for assistance and performing ovariectomies. This work was supported by Cornell University internal funds to D.C.B. and D.C.B. was supported by NIDDK awards R01-DK132264.

Author contributions

Y.J and D.C.B initiated the study. B.M.S, A.M.B, D.L, Y.J, and D.C.B designed and performed the experiments, collected data, and analyzed the results. B.M.S, A.M.B, D.L, and D.C.B wrote the manuscript.

Competing interests

The authors declare no competing interests.

Additional information

Supplementary information The online version contains supplementary material available at https://doi.org/10.1038/s41467-024-50985-8.

Correspondence and requests for materials should be addressed to Daniel C. Berry.

Peer review information *Nature Communications* thanks the anonymous, reviewer(s) for their contribution to the peer review of this work. A peer review file is available.